Reassessing the contribution of the Na^+/H^+ exchanger Nhe3b to Na^+ uptake in zebrafish (*Danio rerio*) using CRISPR/Cas9 gene editing

Alex M. Zimmer[a]*, Khatereh Shir-Mohammadi[a], Raymond W.M. Kwong[b], Steve F. Perry[a]

[a]Department of Biology, University of Ottawa, Ottawa, Ontario, Canada

[b]Department of Biology, York University, Toronto, Ontario, Canada

*Corresponding author:

Alex M. Zimmer
azimmer@uottawa.ca
University of Ottawa
Department of Biology
Gendron Hall
30 Marie Curie Private
Ottawa, ON
Canada K1N 6N5

Abstract

Freshwater fishes absorb Na^+ from their dilute environment using ion-transporting cells. In larval zebrafish (*Danio rerio*), Na^+ uptake is coordinated by (1) Na^+/H^+-exchanger 3b (Nhe3b) and (2) H^+-ATPase-powered electrogenic uptake in H^+-ATPase-rich (HR) cells and by (3) Na^+-Cl^--cotransporter (Ncc) expressed in NCC cells. The present study aimed to better understand the roles of these 3 proteins in Na^+ uptake by larval zebrafish under 'normal' (800 µmol/L) and 'low' (10 µmol/L) Na^+ conditions. We hypothesized that Na^+ uptake would be reduced by CRISPR/Cas9 knockout (KO) of *slc9a3.2* (encoding Nhe3b), particularly in low Na^+ where Nhe3b is believed to play a dominant role. Contrary to this hypothesis, Na^+ uptake was sustained in nhe3b KO larvae under both Na^+ conditions, which led to the exploration of whether compensatory regulation of H^+-ATPase or Ncc was responsible for maintaining Na^+ uptake in nhe3b KO larvae. mRNA expression of the genes encoding H^+-ATPase and Ncc were not altered in nhe3b KO. Moreover, morpholino knockdown of H^+-ATPase, which significantly reduced H^+ flux by HR cells, did not reduce Na^+ uptake in nhe3b KO larvae, nor did rearing larvae in chloride-free conditions, thereby eliminating any driving force for Na^+-Cl^--cotransport via Ncc. Finally, simultaneously treating nhe3b KO larvae with H^+-ATPase morpholino and chloride-free conditions did not reduce Na^+ uptake under normal or low Na^+. These findings highlight the flexibility of the Na^+ uptake system and demonstrate that Nhe3b is expendable to Na^+ uptake in zebrafish and that our understanding of Na^+ uptake mechanisms in this species is incomplete.

Keywords: Compensatory regulation; H^+-ATPase; ionocyte; ion regulation; Na^+-Cl^--cotransporter (Ncc); Rhesus glycoprotein Rhcgb (formerly Rhcg1)

Introduction

For nearly a century, comparative physiologists have sought to determine the mechanisms by which freshwater (FW) fishes absorb ions from their dilute hypoionic environment to counteract passive salt loss. Zebrafish (*Danio rerio*) has emerged as a powerful model for understanding ionoregulatory mechanisms by FW fishes (Hwang et al., 2011; Dymowska et al., 2012; Kumai and Perry, 2012; Guh et al., 2015), owing primarily to its ease of husbandry, short generation time, and amenability to genetic manipulations. A model for ion uptake in zebrafish has been established whereby multiple subtypes of ion-transporting cells (ionocytes) coordinate the absorption of specific ions. Na^+ uptake, in particular, is coordinated by 3 distinct pathways; i) Na^+/H^+ exchange via Slc9a3.2 (Na^+/H^+-exchanger 3b; Nhe3b) expressed in H^+-ATPase-rich (HR) cells, ii) electrogenic Na^+ uptake via a putative Na^+ channel powered by Atp6v1aa (H^+-ATPase) expressed in HR cells and iii) Na^+-Cl^- cotransport by Slc12a10.2 (Na^+-Cl^--cotransporter-like 2; hereafter referred to as Ncc) expressed in NCC cells (Hwang et al., 2011; Dymowska et al., 2012; Hwang and Chou, 2013; Hwang and Lin, 2014; Guh et al., 2015).

Nhe3b was first localized to HR cells of zebrafish using immunohistochemical labelling and *in situ* hybridization (Yan et al., 2007) and its role in Na^+ uptake was supported by a reduction in whole-body Na^+ uptake and HR cell-specific Na^+ accumulation in 4 days post-fertilization (dpf) larvae by treatment with 5-(N-ethyl-N-isopropyl) amiloride (EIPA), a specific inhibitor of NHE (Esaki et al., 2007). Moreover, epithelial Na^+ influx, measured by the scanning ion-selective electrode technique (SIET), was reduced in response to EIPA treatment and in response to antisense morpholino oligonucleotide knockdown (KD) of Nhe3b (Shih et al., 2012). It is important to note, however, that EIPA was also shown to have no inhibitory effect on Na^+ uptake in zebrafish larvae and adults in other studies (Boisen et al., 2003; Kumai and Perry, 2011; Kwong and Perry, 2013; Dymowska et al., 2015). The reductions in epithelial Na^+ gradients that were observed in response to EIPA and Nhe3b KD (Shih et al., 2012) were demonstrated only in larvae reared in a low ambient Na^+ concentration (5 µmol/L). In fact, several studies have demonstrated that *nhe3b* gene expression increases in response to low Na^+ acclimation in zebrafish (Yan et al., 2007; Shih et al., 2012; Lin et al., 2016). An increased role for Nhe3b in low Na^+ is surprising given that NHE function even in "typical" FW (~1 mmol/L Na^+) has been debated on thermodynamic grounds (Parks et al., 2008). However, the thermodynamic constraints of NHE function in FW are believed to be overcome by close association with apical ammonia-transporting

Rhesus (Rh) glycoproteins. In zebrafish, Rhcgb (formerly Rhcg1) is expressed on the apical membrane of HR cells (Nakada et al., 2007; Ito et al., 2013) and is believed to facilitate Na^+/H^+ exchange by binding cytosolic NH_4^+, stripping off H^+, and conducting NH_3 after which it is titrated by H^+ in the apical boundary layer (reviewed by Hwang and Lin, 2014; Wright and Wood, 2009; Wright and Wood, 2012; Zimmer et al., 2017). This arrangement of Nhe3b and Rhcgb, in addition to the presence of cytosolic carbonic anhydrase (Wright and Wood, 2009; Ito et al., 2013), is believed to create an acidic microenvironment in the cytosol and an alkaline microenvironment in the apical boundary layer that provides a sufficient H^+ gradient to drive Na^+/H^+ exchange against a Na^+ concentration gradient. The role of this Rhcgb/Nhe3b metabolon in Na^+ uptake is also supported by the observation that gill *rhcgb* mRNA expression increased in response to low Na^+ conditions (Nakada et al., 2007; Shih et al., 2012) and morpholino KD of Rhcgb reduced epithelial Na^+ influx in 4 dpf larvae reared in low Na^+ (Shih et al., 2012).

The H^+-ATPase model of Na^+ uptake was originally proposed as a more thermodynamically feasible mechanism of Na^+ uptake in FW fishes (Avella and Bornancin, 1989). In larval zebrafish, treatment with the H^+-ATPase inhibitor bafilomycin A1 reduced H^+ flux at HR cells by nearly 80% (Lin et al., 2006) and H^+-ATPase KD resulted in reductions in both epithelial H^+ gradients and whole-body Na^+ content (Horng et al., 2007). Interestingly, this reduction in whole-body Na^+ content in H^+-ATPase morphants (individuals treated with a morpholino) was observed only in larvae reared under low Na^+ (10 µmol/L) conditions, contrary to previous reports suggesting that the role of H^+-ATPase in Na^+ uptake is diminished under low Na^+ conditions and that Nhe3b is the dominant pathway in low Na^+ (Yan et al., 2007; Shih et al., 2012). Treatment with bafilomycin also reduced the accumulation of Na^+ in HR cells (Esaki et al., 2007) and inhibited whole-body Na^+ uptake in zebrafish larvae acclimated to ~800 µmol/L Na^+ (Esaki et al., 2007; Kumai and Perry, 2011; Kwong and Perry, 2013), providing further support for H^+-ATPase-mediated Na^+ uptake in zebrafish. In adult zebrafish, however, the effect of bafilomycin on Na^+ uptake is more equivocal, its effects being dependent on water chemistry and exposure duration (Boisen et al., 2003). The electrogenic apical entry of Na^+, driven by H^+-ATPase, has long been controversial because a homologous epithelial Na channel (ENaC) gene has not been found in the genome of any fish species examined to date (Hwang et al., 2011; Dymowska et al., 2012) and the ENaC-specific blocker phenamil has been demonstrated to reduce Na^+ uptake in FW fishes in some instances (Grosell and Wood, 2002; Reid et al., 2003; Preest et al.,

2005; Brix and Grosell, 2012), but not others (Preest et al., 2005; Dymowska et al., 2014). More recently, the acid-sensing ion channel (ASIC) Asic4b has been implicated as the channel involved in H^+-ATPase-mediated electrogenic Na^+ uptake in rainbow trout (Dymowska et al., 2014) and zebrafish (Dymowska et al., 2015; Zimmer et al., 2018).

In addition to HR cell-mediated Na^+ uptake by Nhe3b and H^+-ATPase, Ncc also is implicated in Na^+ uptake by FW fishes (Hiroi et al., 2008; Wang et al., 2009; Hwang et al., 2011; Dymowska et al., 2012; Hwang and Chou, 2013; Hwang and Lin, 2014; Guh et al., 2015), despite that the function of this electroneutral transporter in FW suffers from some of the same thermodynamic limitations as Nhe3b (Parks et al., 2008). In zebrafish, Ncc is expressed in a subset of cells on the yolk sac epithelium of zebrafish that do not express H^+-ATPase (NCC cells; Kwong et al., 2016; Wang et al., 2009) and treatment with the NCC-specific pharmacological blocker metolazone resulted in a significant reduction in whole-body Na^+ uptake in larvae (Wang et al., 2009), although this blocker also was shown to have no effect on Na^+ uptake in other studies (Esaki et al., 2007; Kwong and Perry, 2013). In response to NCC KD, Na^+ uptake and whole-body Na^+ levels increased in larval zebrafish (Wang et al., 2009; Chang et al., 2013; Kwong and Perry, 2016), likely as a function of increased flux via Nhe3b (Wang et al., 2009; Chang et al., 2013). It is likely, therefore, that Ncc is an important pathway for Na^+ uptake, requiring compensatory changes in Na^+ uptake mechanisms when eliminated via morpholino KD. Moreover, in at least one study, *slc12a10.2* mRNA expression (encoding Ncc) was shown to be upregulated in larval zebrafish in response to low Na^+ acclimation (Lin et al., 2016).

The goal of the present study was to further elucidate the roles of the 3 putative pathways of Na^+ uptake (Nhe3b, H^+-ATPase-mediated, Ncc) under typical ("normal"; 800 µmol/L) and "low" (10 µmol/L) Na^+ conditions using a combination of clustered regularly interspaced palindromic repeats (CRISPR)/CRISPR-associated nuclease 9 (Cas9), morpholino KD, and water chemistry manipulation. In particular, we hypothesized that CRISPR/Cas9 knockout (KO) of *slc9a3.2* (encoding Nhe3b) would result in reduced Na^+ uptake rates specifically under low Na^+ conditions. Alternatively, compensatory regulation might occur in nhe3b KO mutants, such that Na^+ uptake would be maintained by the other two Na^+ uptake pathways (H^+-ATPase-mediated and/or Ncc pathways), as previously described in response to morpholino KD of Nhe3b, Ncc (Wang et al., 2009; Chang et al., 2013) and the cation channel Asic4b (Zimmer et al., 2018) that is thought to be involved in H^+-ATPase-mediated Na^+ uptake in fishes (Dymowska et al., 2014; Dymowska et al., 2015).

Therefore we predicted that if compensatory upregulation of H^+-ATPase and/or Ncc were to occur, H^+-ATPase KD and/or rearing larvae under chloride-free conditions (to limit Na^+-Cl^--cotransport) would result in a reduction in Na^+ uptake in nhe3b KO larvae. The effect of CRISPR/Cas9 KO of *rhcgb* on Na^+ uptake was also assessed and we predicted that if compensatory regulation of Na^+ uptake occurred in nhe3b KO larvae, the same compensatory mechanisms would be upregulated in rhcgb KO larvae as this protein is presumed to be a requisite for Nhe3b-mediated Na^+ uptake in zebrafish. Overall, we found that Na^+ uptake was not reduced in nhe3b or rhcgb KO larvae in normal or low Na^+ conditions and that the maintenance of Na^+ uptake in nhe3b KO larvae did not appear to be a function of compensatory regulation by the H^+-ATPase-mediated or Ncc pathways.

Material and Methods

Zebrafish

Mutant zebrafish (nhe3b KO and rhcgb KO) were generated using CRISPR/Cas9 gene editing and were treated and handled in the same way as wild-type fish. Adult zebrafish (*Danio rerio*), originally purchased from the pet trade, were bred and raised in the University of Ottawa animal holding facilities. Fish were kept in plastic aquaria receiving re-circulating dechloraminated City of Ottawa tap water (in mmol/L: 0.8 Na^+, 0.4 Cl^-, 0.25 Ca^{2+}; pH 7.6) and were maintained at 28 ºC with a photoperiod of 14:10 h light:dark. Fish were bred by placing 2 female and 1 male zebrafish overnight in a plastic container with a perforated bottom insert. The following morning, embryos were collected and were reared in Petri dishes containing 50 mL of reconstituted water that differed in composition depending on the experiment (see below). Embryos were reared at a density of 40 individuals/50 mL in an incubator set to 28 ºC; water was replaced daily. All fish handling and experimental procedures were in accordance with the guidelines of the Canadian Council of Animal Care and were approved by the University of Ottawa Animal Care Committee (protocol BL-1700).

Generation of nhe3b KO and rhcgb KO zebrafish

CRISPR/Cas9 gene editing was used to knock out the expression of *slc9a3.2* (*nhe3b*; NCBI accession: NM_001113479.1) and *rhcgb* (formerly *rhcg1*; NCBI accession: NM_001320382.1). CRISPR/Cas9 single guide RNAs (sgRNAs) were designed using CHOPCHOP (Montague et al., 2014; Labun et al., 2016) and were specific to exon 1 of

slc9a3.2 (TGCATTACATGAGGCTGCTG), upstream of a protospacer-adjacent motif (PAM) (CGG), and to exon 1 of *rhcgb* (GGGCAACTGCTTCGGCTCCA), upstream of a PAM (GGG) (Fig. 1). sgRNAs were synthesized using a cloning-free method described previously (Talbot and Amacher, 2014) but with slight modifications. First, a set of primers was employed to amplify DNA constructs (Table S1) that acted as templates for *in vitro* sgRNA transcription. The constructs were amplified in 50-µL PCR reactions consisting of 250 nmol/L *slc9a3.2* or *rhcgb* template oligo, 250 nmol/L universal template oligo 2, 20 nmol/L forward amplification oligo, 20 nmol/L reverse amplification oligo (Table S1), 200 µmol/L dNTPs, 5 µl 10X ThermoPol buffer (New England Biolabs (NEB), Ipswich, MA, USA), and 0.25 µL Taq (NEB). Reactions started with initial denaturation at 95 ºC for 30 s followed by 35 cycles of 95 ºC for 30 s (denaturation), 55 ºC for 1 min (annealing), and 72 ºC for 45 s (extension), and a final extension at 72 ºC for 10 min. The PCR products were column-purified (QIAGEN, Hilden, Germany) and the size and quality of the resulting PCR constructs were verified by gel electrophoresis. DNA concentration was determined spectrophotometrically (NanoDrop 2000; ThermoFisher, Waltham, MA, USA). The sgRNAs were transcribed from PCR constructs using a HiScribe T7 high yield RNA synthesis kit (NEB) with 200 ng DNA template, following the protocol of the manufacturer. sgRNA size and quality were verified by gel electrophoresis, and RNA concentration was determined spectrophotometrically following purification (RNeasy mini kit, QIAGEN).

Zebrafish codon-optimized Cas9 (pCS2-nls-zCas9-nls) was obtained from Jao et al. (2013) and was used as a template to synthesize Cas9 mRNA. The pCS2-nls-zCas9-nls plasmid was linearized by NotI digestion and purified using a QIAquick purification kit (QIAGEN). Capped nls-zCas9-nls RNA was synthesized using mMESSAGE mMACHINE SP6 kit (Invitrogen, Carlsbad, CA, USA). Following purification (RNeasy Mini kit, QIAGEN), the size and quality of the Cas9 mRNA was checked by gel electrophoresis and Cas9 mRNA concentration was determined spectrophotometrically.

Wild-type zebrafish embryos at the 1-cell stage were injected with 1 nL of injection solution containing 150 pg Cas9 mRNA, 50 pg of *slc9a3.2* or *rhcgb* sgRNA, and 0.01% phenol red (for visualization) suspended in Danieau buffer (in mmol/L: 58 NaCl, 0.7 KCl, 0.4 $MgSO_4$, 0.6 $Ca(NO_3)_2$, and 5.0 Hepes; pH 7.6). At 1 dpf, a subset of embryos was genotyped to determine whether the injections resulted in the generation of mutant embryos. Embryos were euthanized with an overdose of Tris-neutralized tricaine methanesulfonate (MS-222) and DNA was extracted by digesting embryos individually in 20 µL 50 mmol/L NaOH at 95

ºC for 10 min and neutralizing with 2 µL 1 mol/L Tris HCl (pH 8). PCR amplification of the CRISPR target regions of *slc9a3.2* and *rhcgb* was performed in 25 µL reactions containing 200 nmol/L forward and reverse sequencing primers (Table S1), 200 µmol/L dNTPs, 2.5 µL 10 X DreamTaq buffer (Thermofisher), 0.125 µL DreamTaq Hot Start DNA polymerase (ThermoFisher), and 5 µL of DNA digest, with a temperature cycle of 94 ºC for 3 min, 35 cycles of 94 ºC for 30 s, 55 ºC for 1 min, and 72 ºC for 45 s, and a final 72 ºC step for 10 min. Amplified PCR products were sequenced by Sanger Sequencing (Genome Quebec, McGill University, Montreal, Canada) which confirmed that a portion (~80%) of the embryos had a mutated *slc9a3.2* or *rhcgb* gene. The remaining embryos were reared to sexual maturity (60-90 dpf) and mutants in this adult F0 population were identified by clipping a small portion of the caudal fin, and genotyping the fin clip following the same protocol described above for embryos. Identified mutants were outcrossed with wild-type fish to establish an F1 heterozygous line. F1 fish were reared to sexual maturity, genotyped, and heterozygous mutants carrying a 5-bp deletion mutation (nhe3b KO mutants) or 1-bp insertion mutation (rhcgb KO mutants) were used as founders for the KO lines. F1 females and males were intercrossed and F2 homozygous *slc9a3.2* mutants (nhe3b KO) and *rhcgb* mutants (rhcgb KO) were identified by fin clipping and genotyping of adult individuals. A breeding population of approximately 20-30 adult F2 nhe3b KO or rhcgb KO mutants was established and these fish were intercrossed to provide F3 mutants on which all experiments were performed. Note that larvae used in this study were obtained from multiple breeding events using several different wild-type or F2 mutant parents. Null mutations in *slc9a3.2* and *rhcgb* were confirmed via Sanger sequencing and whole-mount immunohistochemistry.

Morpholino KD

Antisense morpholino oligonucleotides (Gene-Tools, LLC, Philomath, OR, USA) were used to knock down the expression of Slc9a3.2 (Nhe3b) or Atp6v1aa (H^+-ATPase) using techniques described in previous studies (Shih et al., 2012; Chang et al., 2013). Briefly, 1-cell stage embryos were injected with 2 or 4 ng of a sham (standard control) morpholino (5'-CCTCTTACCTCAGTTACAATTTATA-3') that has no biological target in zebrafish, 2 ng of a translation-blocking morpholino that targeted the translation start site of *slc9a3.2* (5'-CAGTTGCCCATGTCTACAGCTTGAG-3') and has been validated in a previous study (Chang et al., 2013), or 4 ng of a translation-blocking morpholino that targets the translation start site of *atp6v1aa* (5'-ATCCATCTTGTGTGTTAGAAAACTG-3'; Horng et al., 2007). Atp6v1aa (H^+-ATPase) KD was confirmed using whole-mount immunohistochemistry.

Morpholinos were suspended in Danieau buffer with 0.01% phenol red and heated to 65 º for 10 min prior to injection at a volume of 1 nL/embryo.

Whole-mount immunohistochemistry

Whole-mount immunohistochemistry was used to confirm KO of Nhe3b and Rhcgb in adult gills and KD of H^+-ATPase in larvae. Adult wild-type, nhe3b KO, and rhcgb KO zebrafish were euthanized with an overdose of neutralized MS-222 and gills were removed and fixed overnight in 4% paraformaldehyde (PFA) in phosphate buffered saline (PBS) at 4 ºC. Following fixation, individual gill filaments were removed from the arch to obtain more even and consistent antibody accessibility. Sham and Atp6v1aa morphant larvae were euthanized with neutralized MS-222 overdose and were fixed overnight in 4% PFA in PBS. In both gill filaments and larvae, antigen retrieval was performed by incubating the samples in 150 mmol/L Tris HCl (pH = 9) for 10 min at room temperature, followed by 15 min at 65 ºC. Samples were rinsed in PBS containing 0.1% Tween-20 (PBS-T) 5 times and blocked and permeabilized in PBST containing 3% BSA and 0.8% Triton X-100 for 2 h at room temperature. Gill filaments from wild-type and nhe3b KO fish were probed overnight at 4 ºC with a custom rabbit polyclonal anti-Nhe3b antibody raised against a synthetic peptide corresponding to the C-terminal region of Nhe3b (CEPAADEETPEEKPA; 1:100 dilution; GenScript, Piscataway, NJ, USA) and a commercial mouse monoclonal anti-Na^+/K^+-ATPase antibody (a5; Developmental Studies Hybridoma Bank, University of Iowa, Ames, IA, USA; 1:250 dilution) diluted in PBST containing 3% BSA and 0.8% Triton X-100. Filaments from wild-type and rhcgb KO fish were probed overnight at 4 °C with a rabbit polyclonal anti-Rhcgb antibody raised against amino acid residues 425-488 of Rhcgb (1:100 dilution; Nakada et al., 2007) and the anti-Na^+/K^+-ATPase antibody. Larvae were probed overnight at 4 °C with a rabbit polyclonal anti-H^+-ATPase antibody (AEMPADSGYPAYLGAR; 1:2000 dilution; courtesy of Dr. M. Uchiyama, University of Toyama, Toyama, Japan). Samples were subsequently rinsed in PBST 5 times and incubated with secondary antibodies (1:500 dilution; Alexa-568 conjugated anti-rabbit IgG and/or Alexa-488 conjugated anti-mouse IgG; Invitrogen). Gill filaments and larvae were finally washed 5 times in PBST and mounted in depression slides in SlowFade Gold antifade mounting medium (ThermoFisher). Images were acquired using a scanning confocal laser microscope (A1R+, Nikon Instruments, Melville, NY, USA).

Manipulation of water ion content

Wild-type, mutant, and/or morphant larvae were reared in water containing 500 µmol/L Cl^-, 250 µmol/L Ca^{2+}, 40 µmol/L K^+, and either 800 µmol/L Na^+ ('normal' Na^+) or 10 µmol/L Na^+ ('low' Na^+) (pH = 7.6) that was prepared by adding $CaCl_2$, $MgSO_4 \cdot 7H_2O$, KH_2PO_4, K_2HPO_4, and Na_2SO_4 salts to ultrapure water (Table 1). "Chloride-free" water was achieved by replacing $CaCl_2$ with $CaSO_4$ (Table 1). Water changes were performed daily and pH was adjusted daily as needed by the addition of 0.1 N KOH or H_2SO_4.

Real-time polymerase chain reaction (PCR)

Real-time PCR was used to assess the expression of genes involved in Na^+ uptake in 4 dpf wild-type, nhe3b KO, and rhcgb KO larvae. Larvae were euthanized via an overdose of neutralized MS-222 and 20 larvae were homogenized via sonication in 0.5 mL Trizol (ThermoFisher). RNA was extracted from these homogenates following the protocol of the manufacturer. RNA concentration was determined via spectrophotometry and RNA quality was verified via gel electrophoresis. RNA was treated with DNase (ThermoFisher) prior to cDNA synthesis from 1 µg total RNA using a commercial kit (iScript; Bio-Rad, Hercules, CA, USA). Real-time PCR was performed in 10 µL reactions containing 5 µL SsoFast EvaGreen supermix (Bio-Rad), 500 nmol/L forward and reverse primers (Table S2), and 4 µL cDNA template. No template controls were run in every assay and non-reverse transcribed samples were run for every primer pair. Reaction efficiency for all primer pairs was between 90 and 110%.

Measurement of Na^+ and Cl^- uptake

Na^+ uptake was measured in 4 dpf wild-type, mutant, or morphant larvae reared under various water chemistry conditions; measurements were made under the same conditions under which the larvae were reared. Experiments on mutant or morphant larvae were always run in parallel with wild-type or sham-treated fish. Larvae were transferred to 2-mL centrifuge tubes (12 larvae/tube for 800 µmol/L Na^+ treatments; 2 larvae/tube for 10 µmol/L Na^+ treatments) containing 1.6 mL of respective acclimation water, incubated in a 28 ºC water bath. For larvae reared under 800 µmol/L Na^+, a density of 12 larvae/tube was used in order to minimize radioisotope cost and waste. Larvae were allowed to settle for 30 min, after which ^{22}Na was added to each tube [0.4 µCi for 800 µmol/L Na^+, mean specific activity = 0.34 ± 0.04 cpm/pmol (n = 12); 0.05 µCi for 10 µmol/L Na^+, mean specific activity = 3.41 ± 0.42 cpm/pmol (n = 12)], marking the beginning of the 3 h Na^+ flux period. Initial and final

0.7 mL water samples were collected for gamma radioactivity and [Na^+] analyses and at the end of the flux period, larvae were euthanized, rinsed 4 times in 10 mmol/L NaCl to displace loosely bound $^{22}Na^+$, and then collected as separate samples (2 larvae per sample; n = 1). Gamma radioactivity of larvae and water samples was determined by gamma counting (2470 Wizard2, Perkin Elmer) and [Na^+] of water samples was determined by flame atomic absorption spectrophotometry (Spectra AA 220FS: Varian, Palo Alto, CA).

Cl^- uptake was measured using the same experimental approach described for Na^+ uptake except that $^{36}Cl^-$ was added to each tube (1 mL/tube; 12 fish/tube for all water chemistry conditions; 0.4 µCi/tube). 0.1 mL samples were collected at the beginning and end of a 3 h flux period for scintillation counting and larvae were euthanized and rinsed 4 times in 10 mmol/L NaCl. Larvae were collected in pairs (n = 1) and digested overnight at 65 °C in 50 µL 2 N HNO_3. Digests and water samples were added to 10 mL EcoLume scintillation cocktail (MP Biomedicals, Solon, OH, USA) and incubated for 3 h in the dark to reduce chemiluminescence prior to scintillation counting (LS-6500 scintillation counter, Beckman Coulter, Brea, CA, USA). [Cl^-] of water used in these experiments was measured using a colorimetric assay (Zall et al., 1956). Na^+ and Cl^- uptake rates (pmol/larva/h) were calculated using the following equation:

$$\text{Ion uptake} = R_{larvae}/SA/t/n \quad (1)$$

where R_{larvae} is the total radioactivity (cpm) of the pooled larvae in a sample, SA is the average specific activity of the water (cpm/pmol), t is flux duration (h), and *n* is the number of larvae.

Scanning ion-selective electrode technique (SIET)

SIET was used to measure H^+ fluxes at HR cells on the yolk sac epithelium of wild-type and nhe3b KO larvae treated with sham or H^+-ATPase morpholino. To visualize HR cells under a fluorescent microscope, live larvae were stained with 0.05 mg/mL concanavalin A (conA) conjugated to Alexa 488 (Invitrogen) for 30 min at room temperature. SIET was performed based on methods described previously (Donini and O'Donnell, 2005; Lin et al., 2006). H^+-selective probes were constructed by pulling borosilicate glass capillaries (World Precision Instruments, Sarasota, FL, USA) to a tip diameter of ~5 µm with a micropipette puller (P-2000, Sutter Instrument, Novato, CA, USA) and silanizing the glass pipettes with N,N-Dimethyltrimethylsilylamine (Sigma-Aldrich, St. Louis, MO, USA) on a hot plate covered by a glass Petri dish for 1 h. Pipettes were then back-filled with a solution of 100

mmol/L NaCl and 100 mmol/L sodium citrate (pH 6) and front-filled with a ~100 µm column of H^+ ionophore I cocktail B (Sigma-Aldrich). H^+-selective probes were then calibrated in 'normal' Na^+ water containing 1 mmol/L Hepes buffer and 0.5 mg/L MS-222 (needed to immobilize larvae during measurements) adjusted to pH 6, 7, or 8. The average Nernstian slope obtained from this calibration was 54.1 ± 0.8 mV (n = 4).

Larvae were secured in place in modified Petri dishes described previously (Hughes et al., 2019) containing 'normal' Na^+ water with 1 mmol/L Hepes buffer and 0.5 mg/L MS-222 (pH 7.6). The Petri dish was positioned under a fluorescent dissecting microscope (SMZ 1500, Nikon) and HR cells were identified by Alexa488-conjugated conA staining. The H^+-selective probe was positioned ~5 µm above the surface of HR cells on the lateral side of the yolk sac epithelium and 5 replicate scans with an excursion distance of 20 µm in the z direction, a wait time of 5 s, and measure time of 1 s were performed at each HR cell; 3-5 HR cells were scanned for each fish (n = 1). H^+ flux (pmol/cm^2/s) was calculated using the following equations (Donini and O'Donnell, 2005):

$$\Delta C = C_B * 10^{(\Delta V/S)} - C_B \quad (2)$$

where ΔC is the concentration gradient (pmol/cm^3) between the origin and excursion point, C_B is the average ion concentration (pmol/cm^3) calculated from voltage measured at the origin and excursion points, ΔV is voltage gradient (µV) and S is the slope of the electrode (µV). This concentration gradient was then converted into a flux using Fick's law:

$$H^+ \text{ flux} = D * \Delta C/\Delta x \quad (3)$$

where D is the diffusion coefficient of H^+ (2.09 X 10^{-5} cm^2/s), ΔC is concentration gradient (pmol/cm^3) and Δx is the excursion distance (cm).

Statistical Analyses

All data are presented as means ± s.e.m. and statistical significance was accepted at the $P < 0.05$ level. Two factor comparisons among multiple means were conducted using a two-way ANOVA followed by a Holm-Sidak post-hoc test. In cases where normality or equal variance was not achieved, data were normalized by square or log transformations. Specific details on the statistical analyses and transformations used for each data set are included in the corresponding figure captions. All statistical analyses were conducted with SigmaStat version 3.5 (Systat Software Inc., San Jose, CA, USA).

Results

Na^+ uptake in nhe3b KO and rhcgb KO larvae and the effects of Nhe3b KD

CRISPR/Cas9 sgRNAs were targeted to exon 1 of *slc9a3.2* and *rhcgb* and resulted in 5 bp deletion and 1 bp insertion mutations, respectively (Figs. 1A, B), confirmed by Sanger sequencing (Figs. 1C, D). Both indel mutations were non-sense mutations, resulting in predicted pre-mature stop codons and truncated proteins (Table S3). KO was confirmed at the protein level by whole-mount immunohistochemistry on gill filaments from adult fish. In wild-type filaments, staining with anti-Nhe3b (Figs. 1E, G) and anti-Rhcgb (Figs. 1F, H) antibodies confirmed cell-specific staining that was not co-localized with anti-Na^+/K^+-ATPase (NKA) staining using the a5 antibody (see Material and Methods), a marker for Ca^{2+}-transporting NKA-rich (NaR) cells (Liao et al., 2007). In the KO larvae, staining of the respective antibody was absent, though NKA staining was still present (Figs. 1E, F). Using the same Nhe3b antibody, we were unsuccessful in visualizing Nhe3b staining in larvae or a band of the appropriate size in western blots; numerous western blots using an array of conditions repeatedly yielded a single non-specific band of approximately 45 kDa that was retained in the KOs (data not shown).

An overall effect of Na^+ level on Na^+ uptake by 4 dpf larvae of all 3 genotypes was observed whereby Na^+ uptake was lower in larvae that were reared and assayed in 10 µmol/L Na^+ relative to the 800 µmol/L Na^+ treatment (Fig. 2). Na^+ uptake between 4 dpf wild-type and nhe3b KO larvae was not significantly different, however Na^+ uptake in rhcgb KO larvae was significantly greater than wild-type and nhe3b KO larvae, indicated by an overall effect of genotype across Na^+ levels (Fig. 2).

Similar to the effect of *nhe3b* KO, Nhe3b KD had no effect on Na^+ uptake in wild-type larvae at either Na^+ level (Fig. 3). Importantly, as a control, the Nhe3b morpholino was injected into nhe3b KO larvae (Fig. 3) in order to ensure that any effect of the morpholino was not recapitulated in the mutant line lacking Nhe3b protein. We found this to be an important control in the use of a different Nhe3b morpholino (Fig. S1; see Discussion). The elevation in Na^+ uptake observed in rhcgb KO larvae (Fig. 2) was not affected by Nhe3b KD (Fig. 3). Overall, Nhe3b loss of function via CRISPR/Cas9 KO or morpholino KD did not result in alterations in Na^+ uptake nor did it alter the pattern of response in the rhcgb KO larvae.

Expression of genes involved in Na^+ uptake

In order to determine whether compensatory regulation occurred in nhe3b KO and rhcgb KO larvae, whole-body gene expression of genes involved in Na^+ uptake was measured. Expression of *slc9a3.2* (encoding Nhe3b) was significantly greater in 4 dpf larvae reared in 10 µmol/L Na^+, relative to those reared in 800 µmol/L Na^+, across all genotypes; there were no significant differences in *slc9a3.2* gene expression among the genotypes (Fig. 4A). The expression of *atp6v1aa* (encoding H^+-ATPase) was not significantly influenced by genotype or Na^+ level (Fig. 4B). Larvae experiencing rhcgb KO displayed significantly lower *asic4b* expression compared to wild-type and nhe3b KO larvae, which were not significantly different from one another; *asic4b* expression was not affected by Na^+ level (Fig. 4C). *slc12a10.2* (encoding Ncc) expression was not significantly different across genotypes or Na^+ level (Fig. 4D).

Effects of *nhe3b* KO on H^+ secretion and Cl^- uptake

Compensatory regulation of Na^+ uptake by H^+-ATPase and Ncc was also assessed at the physiological level by measuring H^+ flux and Cl^- uptake. H^+ flux at the surface of HR cells (Fig. 5A) of larvae reared and assayed in 800 µmol/L Na^+ was not significantly different between wild-type and nhe3b KO larvae (Fig. 5B), however, there was an overall inhibitory effect of Atp6v1aa (H^+-ATPase) KD on H^+ flux by HR cells (Fig. 5B); successful KD was confirmed by immunohistochemistry (Figs. 5C, D).

Cl^- uptake was significantly increased in the nhe3b KO larvae in comparison to wild-types; Na^+ level had no effect on Cl^- uptake (Fig. 6).

Na^+ uptake in response to H^+-ATPase KD **and chloride-free conditions**

To further probe the mechanisms promoting compensatory regulation of Na^+ uptake in nhe3b KO larvae, larvae were subjected to H^+-ATPase KD and chloride-free rearing conditions. Interestingly, while in prior experiments there were no differences in Na^+ uptake rates between wild-type and nhe3b KO larvae (Figs. 1, 2), the following experiments revealed a stimulatory effect of *nhe3b* KO on Na^+ uptake, which was present only in some instances and did not appear to depend on Na^+ level (Figs. 7A, 7B, 8A, 9B). In 800 µmol/L Na^+, H^+-ATPase KD resulted in a stimulation of Na^+ uptake in 4 dpf wild-type larvae, while this effect was absent in nhe3b KO larvae (Fig. 7A). This stimulatory effect of H^+-ATPase KD also was absent in 10 µmol/L Na^+ (Fig. 7B). Rearing and assaying larvae in chloride-free

conditions had no effect on Na^+ uptake regardless of genotype or Na^+ level (Fig. 8). Most surprisingly, Na^+ uptake in nhe3b KO larvae experiencing H^+-ATPase KD that were reared (and assayed) in chloride-free conditions was not reduced relative to Na^+ uptake by wild-type larvae treated with sham morpholino and reared under control chloride conditions at either Na^+ level (Fig. 9). In fact, under 'low' Na^+ conditions, Na^+ uptake was highest in this group experiencing a functional ablation of all 3 putative Na^+ uptake pathways (nhe3b KO, H^+-ATPase KD, chloride-free conditions).

Discussion

In the present study, we aimed to further elucidate the mechanisms of Na^+ uptake utilized by larval zebrafish, particularly under low Na^+ conditions. Using CRISPR/Cas9 gene editing we hypothesized that loss of Nhe3b or Rhcgb, an ammonia-transporting protein thought to be integral to the thermodynamic operation of Nhe3b in FW (Wright and Wood, 2009), would result in a reduced capacity to absorb Na^+ from a dilute environment. Contrary to our predictions, nhe3b and rhcgb KO larvae maintained Na^+ uptake at the same or greater rate as wild-type larvae, even under low Na^+ conditions (Fig. 2). This led us to explore the possibility of compensatory regulation by alternate Na^+ uptake pathways in nhe3b KO larvae, previously shown to occur after morpholino KD of Nhe3b, Ncc (Chang et al., 2013), and Asic4b (Zimmer et al., 2018). Such compensatory regulation is believed to be a fairly widespread consequence of gene KO in zebrafish (El-Brolosy and Stainier, 2017). Through several experiments, we concluded that neither the H^+-ATPase-mediated nor Ncc pathways of Na^+ uptake compensated for the loss of Nhe3b, and that Na^+ uptake persisted when all 3 putative pathways for Na^+ uptake were targeted simultaneously.

The role of Nhe3b in Na^+ uptake by zebrafish

In zebrafish and other fishes, Nhe3b and Rhcgb are believed to associate as part of a functional metabolon that alleviates the presumed thermodynamic constraints on electroneutral Na^+/H^+ exchange in FW (Wright and Wood, 2009; Wu et al., 2010; Dymowska et al., 2012; Ito et al., 2013; Guh et al., 2015). Surprisingly, in zebrafish, the contribution of Nhe3b to Na^+ uptake increased in response to acclimation to low Na^+ (Lin et al., 2016; Shih et al., 2012; Yan et al., 2007; Fig. 4A), a condition which would theoretically exacerbate the thermodynamic limitations of Nhe3b function. However, the expression of *rhcgb* also appears to be increased in response to low Na^+ acclimation (Nakada et al., 2007; Shih et al., 2012), further indicating the potential importance of Rhcgb in maintaining Na^+ uptake via

Nhe3b. Based on these findings, we had hypothesized that Na^+ uptake would be limited, particularly under low Na^+ conditions, in nhe3b and rhcgb KO larvae. However, neither KO resulted in a reduction in Na^+ uptake under normal (800 µmol/L) or low (10 µmol/L) Na^+ (Fig. 2). Notably, the mean specific activity (SA; see Material and Methods) in our study was an order of magnitude lower in the 800 µmol/L Na^+ experiments than in the 10 µmol/L experiments. To our knowledge, the influence of SA on ion uptake rates in fish has never been tested directly. Regardless, the most important comparisons made in the present study were those made within a Na^+ level treatment, and therefore the potentially confounding influence of SA on Na^+ uptake would not affect the interpretation of our results. In previous work, morpholino KD of Nhe3b and Rhcgb reduced Na^+ uptake by zebrafish larvae under low Na^+ (Shih et al., 2012) and low pH (Kumai and Perry, 2011) acclimation conditions.

Using the same Nhe3b morpholino and dose that were used in the present study, Shih et al. (2012) demonstrated that epithelial Na^+ influx (measured by SIET) was reduced in larvae reared in 5 µmol/L Na^+. While we were unable to replicate this effect (Fig. 3), it is possible that the differences between these studies reflects the method with which Na^+ uptake was assessed. It is conceivable that localized reductions in epithelial Na^+ influx in Nhe3b morphants measured by SIET (Shih et al., 2012) cannot be detected when Na^+ uptake is measured at the whole-body level. Regardless, the results obtained with Nhe3b KD in the current study were consistent with the phenotype of nhe3b KO mutants. Moreover, there were no off-target effects of the morpholino when injected into nhe3b KO embryos, an important control for morpholino experiments (Zimmer et al., 2019). A caveat to our results is that we were unable to confirm Nhe3b KD because the Nhe3b antibody failed to detect Nhe3b expression in whole-mount immunostaining or western blotting of larvae, despite working well in adult gills (Fig. 1E). However, given that the same dose of this Nhe3b morpholino (2 ng/embryo) was shown to reduce Nhe3b expression in a previous study (Chang et al., 2013), it seems likely that successful KD also was achieved in the current study. Nevertheless, it is clear that zebrafish larvae do not require Nhe3b to sustain whole-body Na^+ uptake under normal or low Na^+ conditions.

Nhe3b also was proposed to contribute to Na^+ uptake under acidic conditions. Kumai and Perry (2011) found that KD of Nhe3b using a different morpholino than that used in the present study and by Shih et al. (2012) resulted in a significant reduction in Na^+ uptake when larvae were reared in pH 4 and acutely transferred to circumneutral pH at 4 dpf. In initial experiments, we employed the morpholino used by Kumai and Perry (2011) to knock down

Nhe3b and found a nearly 50% reduction in Na^+ uptake in wild-type and rhcgb KO larvae reared and assayed in low Na^+ (Fig. S1). However, this same effect was recapitulated in nhe3b KO larvae lacking Nhe3b (Fig. S1), indicating that this morpholino exhibits off-target effects on Na^+ uptake that cannot be attributed to Nhe3b KD. Moreover, we discovered that the Rhcgb morpholino employed by Kumai and Perry (2011) was mistakenly designed to target (*rhcg-like 1*; *rhcgl1*, formerly *rhcg2*), a different *rhcg* paralog for which we currently have little information in terms of localization and function. Therefore, it appears that the contribution of the Rhcgb/Nhe3b metabolon to Na^+ uptake under acidic conditions remains equivocal. Indeed, in other studies, mRNA expression of *slc9a3.2* was found to be decreased in the gills of adult zebrafish acclimated to acidic conditions (Yan et al., 2007; Chang et al., 2013).

Compensatory regulation in gene loss of function approaches

In response to gene KD or KO, compensatory regulation of paralogous or functionally related genes has been documented in a number of studies on zebrafish (see El-Brolosy and Stainier, 2017), such that null mutations may not always result in any obvious phenotype (Balciunas, 2018). The mechanism(s) by which this compensatory regulation occurs is not yet clear, but may involve signaling from mutant mRNA (El-Brolosy et al., 2019), at least in the case of gene KO. In zebrafish, compensatory regulation has been demonstrated in response to morpholino KD of several genes involved in Na^+ uptake. For example, KD of Nhe3b in zebrafish reduced whole-body Na^+ content in 2 - 4 dpf larvae, but a concomitant increase in the density of NCC cells reversed this effect by 5 dpf (Chang et al., 2013). While NCC cell density was not assessed in nhe3b KO larvae, it is possible that Na^+ flux via Ncc was elevated given that Cl^- uptake rate was significantly greater in nhe3b KO larvae, compared to wild-types (Fig. 6), although *slc12a10.2* mRNA expression was unchanged (Fig. 4). Notably, however, Cl^- uptake was unaffected by Na^+ levels in wild-type or nheb3 KO larvae, suggesting that Cl^- uptake is mediated by non-Ncc pathways, such as Slc26a anion exchangers (Perry et al., 2009; Bayaa et al., 2009), given that the driving force for Na^+-Cl^--cotransport would be minimal under low Na^+ conditions. Compensatory regulation also occurred in response to Ncc KD in zebrafish. Ncc morphants displayed a significant reduction in Cl^- uptake, but a stimulation of Na^+ uptake (Wang et al., 2009; Kwong and Perry, 2016), indicating compensation from alternate Na^+ uptake pathways. Indeed, *nhe3b* mRNA expression (Wang et al., 2009) and HR cell density (Chang et al., 2013) were increased in Ncc morphant zebrafish by 4 dpf. In addition, KD of Asic4b, an acid-sensing cation channel

that may be involved in H^+-ATPase-mediated Na^+ uptake in zebrafish (Dymowska et al., 2015), resulted in an increase in the density of HR cells and increased mRNA expression of *nhe3b* and *slc12a10.2*, which may have served to maintain normal rates of Na^+ uptake (Zimmer et al., 2018). Clearly, the phenomenon of compensatory regulation is widespread in the Na^+ uptake system of zebrafish, which led to the hypothesis in the current study that Na^+ uptake by nhe3b KO larvae may be sustained by the H^+-ATPase and/or Ncc-mediated pathways.

Compensatory regulation does not account for maintenance of Na^+ uptake by nhe3b KO larvae

None of the approaches used to assess the contribution of H^+-ATPase to Na^+ uptake in nhe3b KO larvae revealed compensatory regulation from this pathway. mRNA expression of *atp6v1aa* was not elevated in nhe3b KO larvae or rhcgb KO larvae (Fig. 4B), and H^+ flux at HR cells was not significantly elevated in nhe3b KO larvae (Fig. 5B), which would have indicated an increase in H^+-ATPase activity. Furthermore, KD of H^+-ATPase did not significantly reduce Na^+ uptake in nhe3b KO larvae under normal or low Na^+ conditions (Fig. 7), despite a clear reduction in H^+ flux by HR cells, at least under normal Na^+ conditions (Fig. 4B). In fact, Na^+ uptake was stimulated by H^+-ATPase KD in wild-type larvae, but not nhe3b KO larvae, under normal conditions (Fig. 7A). To our knowledge, this is the first demonstration of a stimulatory effect of H^+-ATPase KD on Na^+ uptake. The mechanisms responsible for the stimulation of Na^+ uptake in Atp6v1aa morphants are unclear but possibilities include increased expression of Ncc, similar to the results of KD of gcm2, a transcription factor that regulates the proliferation of HR cells (Chang et al., 2013; Kwong and Perry, 2016), or an increase in Nhe3b expression given that Na^+ uptake was not stimulated by H^+-ATPase KD in nhe3b KO larvae. However, H^+ flux in wild-type and nhe3b KO larvae treated with H^+-ATPase morpholino did not differ from one another (Fig. 5B), which might indicate that Nhe3b does not supplant the function of H^+-ATPase in wild-type H^+-ATPase morphants.

Cl^- uptake increased significantly in response to nhe3b KO (Fig. 6), potentially indicating compensatory regulation by Ncc, as was demonstrated for Nhe3b KD (Chang et al., 2013). However, rearing larvae under chloride-free conditions, achieved by replacing Cl^- with SO_4^{2-}, had no effect on Na^+ uptake by wild-type or nhe3b KO larvae, regardless of Na^+ level. In a previous study, chloride removal was demonstrated to have no effect on Na^+

uptake under 'normal' Na^+ conditions in 4 dpf larvae (Kwong and Perry, 2016), although a nearly 50% reduction in Na^+ uptake was observed in 3 dpf larvae in another study (Kwong and Perry, 2013). Chloride-free conditions have also been shown to attenuate increases in Na^+ uptake observed during recovery from acute acid exposure (Kwong and Perry, 2016) and in response to morpholino KD of Claudin-b, a tight junction protein (Kwong and Perry, 2013). Importantly, the increase in Na^+ uptake observed in both acute acid treatment and Claudin-b KD were attributed to Ncc (Kwong and Perry, 2013; Kwong and Perry, 2016), suggesting that chloride-free treatment is an effective way to assess the contribution of Ncc to Na^+ uptake. Therefore, despite an increase in Cl^- uptake, it does not appear that Ncc plays a significant role in sustaining Na^+ uptake in nhe3b KO larvae.

Given the apparent flexibility of the Na^+ uptake system of zebrafish, it is conceivable that even after Na^+ uptake is reduced to only one of the 3 putative pathways (e.g. nhe3b KO larvae experiencing H^+-ATPase KD), Na^+ uptake can continue at normal rates. Therefore, an experiment whereby all 3 pathways were targeted simultaneously was conducted. Surprisingly, in nhe3b KO larvae treated with H^+-ATPase morpholino and reared and assayed under chloride-free conditions, Na^+ uptake was not reduced relative to wild-type larvae treated with sham morpholino and reared and assayed under control chloride conditions (Fig. 9). How can Na^+ uptake be sustained in the absence of Nhe3b and H^+-ATPase and in the absence of a driving force (Cl^--free) for Na^+-Cl^--cotransport? First, it is possible that compensatory regulation of another *nhe* paralog could supplant the function of *nhe3b*. Indeed, *nhe2* is expressed in the gills of adult zebrafish (Yan et al., 2007) and this gene is thought to be an important component of Na^+ uptake in rainbow trout (Zimmer et al., 2010; Zimmer et al., 2017b). However, no study to our knowledge has localized its expression to ionocytes of larval zebrafish. Second, it is possible that a Na^+ channel might function in the absence of a H^+ electromotive force generated by H^+-ATPase. Recently, Esbaugh et al. (2019) suggested that NKA isoform switching might allow NKA to function at exceedingly low levels of intracellular Na^+ (~10 µmol/L) by changing the stoichiometry of the pump, thereby lowering its activation energy. Indeed, the expression of one particular paralog, *atp1a1a.5*, that is predicted to have a 1:1 Na^+:K^+ stoichiometry and therefore lower activation energy, was increased in response to low Na^+ (<10 µmol/L) acclimation in the gills of adult zebrafish (Esbaugh et al., 2019). Thus, it is possible that a concentration gradient between the surrounding environment and cytosol could be maintained such that a Na^+ channel alone could transport Na^+ in the absence of H^+-ATPase. Third, if SO_4^{2-} can substitute for Cl^- via

Ncc, perhaps Ncc can still function to absorb Na^+ under the chloride-free conditions used in the present study. However, as discussed earlier, this method of chloride removal has been effective in reducing Na^+ uptake in previous work under conditions in which Ncc function is upregulated (Kwong and Perry, 2013; Kwong and Perry, 2016) and the hydrated ionic radius of SO_4^{2-} (0.242 nm) is substantially larger than that of Cl^- (0.180 nm) (Marcus, 1988), further suggesting that it is unlikely that Na^+ is absorbed as Na^+-SO_4^{2-}-co-transport via Ncc. Finally, there may be an alternative pathway for Na^+ uptake that has not yet been discovered in FW fishes.

Conclusions and perspectives

Despite a nearly century-long effort to elucidate the mechanisms of Na^+ uptake by FW fishes, there are many aspects of this vital physiological function that remain unclear. Even with powerful techniques such as CRISPR/Cas9 gene editing, the apparent flexibility and plasticity of the Na^+ uptake system make uncovering its mechanisms challenging. The present study unequivocally demonstrated that Nhe3b is expendable to Na^+ uptake in larval zebrafish, but the pathways supplanting the function of this protein, especially in low Na^+ where its role is increased, remain unclear. We hypothesized that ablating the function of the other two pathways of Na^+ uptake (H^+-ATPase-mediated and Ncc) in nhe3b KO larvae would reveal mechanisms of compensatory regulation in response to nhe3b KO. However, these experiments instead pointed towards the possibility that an unknown pathway for Na^+ uptake may exist in zebrafish and that this may be an important avenue to explore in future research.

Acknowledgements

The authors thank Christine Archer, Vishal Saxena, and Bill Fletcher of the University of Ottawa Animal Care and Veterinarian Services. This research was supported by NSERC Discovery grants # G13017 to SFP, and #05984 to RWMK. RWMK was also supported by the Canada Research Chairs Program. AMZ was supported by an NSERC Post-Doctoral Fellowship.

References

Avella, M. and Bornancin, M. (1989). A new analysis of ammonia and sodium transport through the gills of the freshwater rainbow trout (*Salmo gairdneri*). *J. Exp. Biol.* **175**, 155–175.

Balciunas, D. (2018). Fish mutant, where is thy phenotype? *PLoS Genet.* **14**, e1007197.

Bayaa, M., Vulesevic, B., Esbaugh, A., Braun, M., Ekker, M. E., Grosell, M. and Perry, S. F. (2009). The involvement of SLC26 anion transporters in chloride uptake in zebrafish (*Danio rerio*) larvae. *J. Exp. Biol.* **212**, 3283–3295.

Boisen, A. M. Z., Amstrup, J., Novak, I. and Grosell, M. (2003). Sodium and chloride transport in soft water and hard water acclimated zebrafish (*Danio rerio*). *Biochim. Biophys. Acta Biomembr.* **1618**, 207–218.

Brix, K. V. and Grosell, M. (2012). Comparative characterization of Na^+ transport in *Cyprinodon variegatus variegatus* and *Cyprinodon variegatus hubbsi*: a model species complex for studying teleost invasion of freshwater. *J. Exp. Biol.* **215**, 1199–1209.

Chang, W. J., Wang, Y. F., Hu, H. J., Wang, J. H., Lee, T. H. and Hwang, P. P. (2013). Compensatory regulation of Na^+ absorption by Na^+/H^+ exchanger and Na^+-Cl^- cotransporter in zebrafish (*Danio rerio*). *Front. Zool.* **10**, 1–12.

Donini, A. and O'Donnell, M. J. (2005). Analysis of Na^+, Cl^-, K^+, H^+ and NH_4^+ concentration gradients adjacent to the surface of anal papillae of the mosquito *Aedes aegypti*: application of self-referencing ion-selective mi. *J. Exp. Biol.* **208**, 603–610.

Dymowska, A. K., Hwang, P. P. and Goss, G. G. (2012). Structure and function of ionocytes in the freshwater fish gill. *Respir. Physiol. Neurobiol.* **184**, 282–292.

Dymowska, A. K., Schultz, A. G., Blair, S. D., Chamot, D. and Goss, G. G. (2014). Acid-sensing ion channels are involved in epithelial Na^+ uptake in the rainbow trout *Oncorhynchus mykiss*. *Am. J. Physiol. Cell Physiol.* **307**, C255–C265.

Dymowska, A. K., Boyle, D., Schultz, A. G. and Goss, G. G. (2015). The role of acid-sensing ion channels in epithelial Na^+ uptake in adult zebrafish (*Danio rerio*). *J. Exp. Biol.* **218**, 1244–1251.

El-Brolosy, M. A. and Stainier, D. Y. R. (2017). Genetic compensation: A phenomenon in search of mechanisms. *PLoS Genet.* **13**, 1–17.

El-Brolosy, M. A., Kontarakis, Z., Rossi, A., Kuenne, C., Guenther, S., Fukuda, N., Kikhi, K., Boezio, G. L. M., Takacs, C., Lai, S.-L., et al. (2019). Genetic compensation is triggered by mutant mRNA degradation. *Nature* **568**, 328153.

Esaki, M., Hoshijima, K., Kobayashi, S., Fukuda, H., Kawakami, K. and Hirose, S. (2007). Visualization in zebrafish larvae of Na^+ uptake in mitochondria-rich cells whose differentiation is dependent on *foxi3a*. *Am. J. Physiol. Regul. Integr. Comp. Physiol.* **292**, R470–R480.

Esbaugh, A. J., Brix, K. V and Grosell, M. (2019). Na^+ K^+ ATPase isoform switching in zebrafish during transition to dilute freshwater habitats. *Proc. R. Soc. B* **286**, 20190630.

Grosell, M. and Wood, C. M. (2002). Copper uptake across rainbow trout gills: mechanisms of apical entry. *J. Exp. Biol.* **205**, 1179–1188.

Guh, Y.-J., Lin, C.-H. and Hwang, P.-P. (2015). Osmoregulation in zebrafish: ion transport mechanisms and functional regulation. *EXCLI J.* **14**, 627–659.

Hiroi, J., Yasumasu, S., McCormick, S. D., Hwang, P.-P. and Kaneko, T. (2008). Evidence for an apical Na-Cl cotransporter involved in ion uptake in a teleost fish. *J. Exp. Biol.* **211**, 2584–2599.

Horng, J.-L., Lin, L.-Y., Huang, C.-J., Katoh, F., Kaneko, T. and Hwang, P.-P. (2007). Knockdown of V-ATPase subunit A (*atp6v1a*) impairs acid secretion and ion balance in zebrafish (*Danio rerio*). *Am. J. Physiol. Regul. Integr. Comp. Physiol.* **292**, R2068--2076.

Hughes, M. C., Zimmer, A. M. and Perry, S. F. (2019). The role of internal convection in respiratory gas transfer and aerobic metabolism in larval zebrafish (*Danio rerio*). *Am. J. Physiol. Regul. Integr. Comp. Physiol.* **316**, R255--R264.

Hwang, P.-P. and Chou, M.-Y. (2013). Zebrafish as an animal model to study ion homeostasis. *Pflügers Arch.* **465**, 1233–1247.

Hwang, P. and Lin, L. Y. (2014). Gill ion transport, acid-base regulation and nitrogen excretion. In *The physiology of fishes* (eds. Evans, D. H., Claiborne, J. B., and Currie, S.), pp. 205–233. Boca Raton: CRC Press.

Hwang, P.-P., Lee, T.-H. and Lin, L.-Y. (2011). Ion regulation in fish gills: recent progress in the cellular and molecular mechanisms. *Am. J. Physiol. Regul. Integr. Comp. Physiol.* **301**, R28–R47.

Ito, Y., Kobayashi, S., Nakamura, N., Miyagi, H., Esaki, M., Hoshijima, K. and Hirose, S. (2013). Close association of carbonic anhydrase (CA2a and CA15a), Na^+/H^+ exchanger (Nhe3b), and ammonia transporter Rhcg1 in zebrafish ionocytes responsible for Na^+ uptake. *Front. Physiol.* **4**, 59.

Jao, L.-E., Wente, S. R. and Chen, W. (2013). Efficient multiplex biallelic zebrafish genome editing using a CRISPR nuclease system. *Proc. Natl. Acad. Sci.* **110**, 13904–13909.

Kumai, Y. and Perry, S. F. (2011). Ammonia excretion via Rhcg1 facilitates Na^+ uptake in larval zebrafish, *Danio rerio*, in acidic water. *Am. J. Physiol. Regul. Integr. Comp. Physiol.* **301**, R1517–R1528.

Kumai, Y. and Perry, S. F. (2012). Mechanisms and regulation of Na^+ uptake by freshwater fish. *Respir. Physiol. Neurobiol.* **184**, 249–256.

Kwong, R. W. M. and Perry, S. F. (2013). The tight junction protein claudin-b regulates epithelial permeability and sodium handling in larval zebrafish, *Danio rerio*. *Am. J. Physiol. Regul. Integr. Comp. Physiol.* **304**, R504--R513.

Kwong, R. W. M. and Perry, S. F. (2016). A role for sodium-chloride cotransporters in the rapid regulation of ion uptake following acute environmental acidosis: new insights from the zebrafish model. *Am. J. Physiol. Cell Physiol.* **311**, C931--C941.

Kwong, R. W. M., Kumai, Y. and Perry, S. F. (2016). Neuroendocrine control of ionic balance in zebrafish. *Gen. Comp. Endocrinol.* **234**, 40–46.

Labun, K., Montague, T. G., Gagnon, J. A., Thyme, S. B. and Valen, E. (2016). CHOPCHOP v2: a web tool for the next generation of CRISPR genome engineering. *Nucleic Acids Res.* **44**, W272--W276.

Liao, B. K., Deng, A. N., Chen, S. C., Chou, M. Y. and Hwang, P. P. (2007). Expression and water calcium dependence of calcium transporter isoforms in zebrafish gill mitochondrion-rich cells. *BMC Genomics* **8**, 1–13.

Lin, L.-Y., Horng, J.-L., Kunkel, J. G. and Hwang, P.-P. (2006). Proton pump-rich cell

secretes acid in skin of zebrafish larvae. *Am. J. Physiol. Cell Physiol.* **290**, C371--C378.

Lin, C. H., Hu, H. J. and Hwang, P. P. (2016). Cortisol regulates sodium homeostasis by stimulating the transcription of sodium-chloride transporter (NCC) in zebrafish (*Danio rerio*). *Mol. Cell. Endocrinol.* **422**, 93–102.

Marcus, Y. (1988). Ionic radii in aqueous solutions. *Chem. Rev.* **88**, 1475–1498.

Montague, T. G., Cruz, J. M., Gagnon, J. A., Church, G. M. and Valen, E. (2014). CHOPCHOP: A CRISPR/Cas9 and TALEN web tool for genome editing. *Nucleic Acids Res.* **42**, 401–407.

Nakada, T., Hoshijima, K., Esaki, M., Nagayoshi, S., Kawakami, K. and Hirose, S. (2007). Localization of ammonia transporter Rhcg1 in mitochondrion-rich cells of yolk sac, gill, and kidney of zebrafish and its ionic strength-dependent expression. *Am. J. Physiol. Regul. Integr. Comp. Physiol.* **293**, R1743–R1753.

Parks, S. K., Tresguerres, M. and Goss, G. G. (2008). Theoretical considerations underlying Na^+ uptake mechanisms in freshwater fishes. *Comp. Biochem. Physiol. C* **148**, 411–418.

Perry, S. F., Vulesevic, B., Grosell, M. and Bayaa, M. (2009). Evidence that SLC26 anion transporters mediate branchial chloride uptake in adult zebrafish (*Danio rerio*). *Am. J. Physiol. Regul. Integr. Comp. Physiol.* **297**, 988–997.

Preest, M. R., Gonzalez, R. J. and Wilson, R. W. (2005). A pharmacological examination of Na^+ and Cl^- transport in two species of freshwater fish. *Physiol. Biochem. Zool.* **78**, 259–272.

Reid, S. D., Hawkings, G. S., Galvez, F. and Goss, G. G. (2003). Localization and characterization of phenamil-sensitive Na^+ influx in isolated rainbow trout gill epithelial cells. *J. Exp. Biol.* **206**, 551–559.

Shih, T.-H., Horng, J.-L., Liu, S.-T., Hwang, P.-P. and Lin, L.-Y. (2012). Rhcg1 and NHE3b are involved in ammonium-dependent sodium uptake by zebrafish larvae acclimated to low-sodium water. *Am. J. Physiol. Regul. Integr. Comp. Physiol.* **302**, R84--R93.

Talbot, J. C. and Amacher, S. L. (2014). A streamlined CRISPR pipeline to reliably generate zebrafish frameshifting alleles. *Zebrafish* **11**, 583–585.

Wang, Y. F., Tseng, Y. C., Yan, J. J., Hiroi, J. and Hwang, P. P. (2009). Role of SLC12A10.2, a Na-Cl cotransporter-like protein, in a Cl uptake mechanism in zebrafish (*Danio rerio*). *Am. J. Physiol. Regul. Integr. Comp. Physiol.* **296**, R1650--R1660.

Wright, P. A. and Wood, C. M. (2009). A new paradigm for ammonia excretion in aquatic animals: role of Rhesus (Rh) glycoproteins. *J. Exp. Biol.* **212**, 2303–2312.

Wright, P. A. and Wood, C. M. (2012). Seven things fish know about ammonia and we don't. *Respir. Physiol. Neurobiol.* **184**, 231–240.

Wu, S.-C., Horng, J.-L., Liu, S.-T., Hwang, P.-P., Wen, Z.-H., Lin, C.-S. and Lin, L.-Y. (2010). Ammonium-dependent sodium uptake in mitochondrion-rich cells of medaka (*Oryzias latipes*) larvae. *Am. J. Physiol. Cell Physiol.* **298**, C237--C250.

Yan, J.-J., Chou, M.-Y., Kaneko, T. and Hwang, P.-P. (2007). Gene expression of Na^+/H^+ exchanger in zebrafish H^+-ATPase-rich cells during acclimation to low-Na^+ and acidic environments. *Am. J. Physiol. Cell Physiol.* **293**, C1814-23.

Zall, D. M., Fisher, D. and Garner, M. Q. (1956). Photometric determination of chlorides in water. *Anal. Chem.* **28**, 1665–1668.

Zimmer, A. M., Nawata, C. M. and Wood, C. M. (2010). Physiological and molecular analysis of the interactive effects of feeding and high environmental ammonia on branchial ammonia excretion and Na^+ uptake in freshwater rainbow trout. *J. Comp. Physiol. B* **180**, 1191–1204.

Zimmer, A. M., Wright, P. A. and Wood, C. M. (2017a). Ammonia and urea handling by early life stages of fishes. *J Exp Biol* **220**, 3843–3855.

Zimmer, A. M., Wilson, J. M., Wright, P. A., Hiroi, J. and Wood, C. M. (2017b). Different mechanisms of Na^+ uptake and ammonia excretion by the gill and yolk sac epithelium of early life stage rainbow trout. *J. Exp. Biol.* **220**, 775–786.

Zimmer, A. M., Dymowska, A. K., Kumai, Y., Goss, G. G., Perry, S. F. and Kwong, R. W. M. (2018). Assessing the role of the acid-sensing ion channel ASIC4b in sodium uptake by larval zebrafish. *Comp. Biochem. Physiol. A* **226**, 1–10.

Zimmer, A. M., Pan, Y. K., Chandrapalan, T., Kwong, R. W. M. and Perry, S. F. (2019). Loss-of-function approaches in comparative physiology: is there a future for knockdown experiments in the era of genome editing? *J. Exp. Biol.* **222**, jeb175737.

Figures

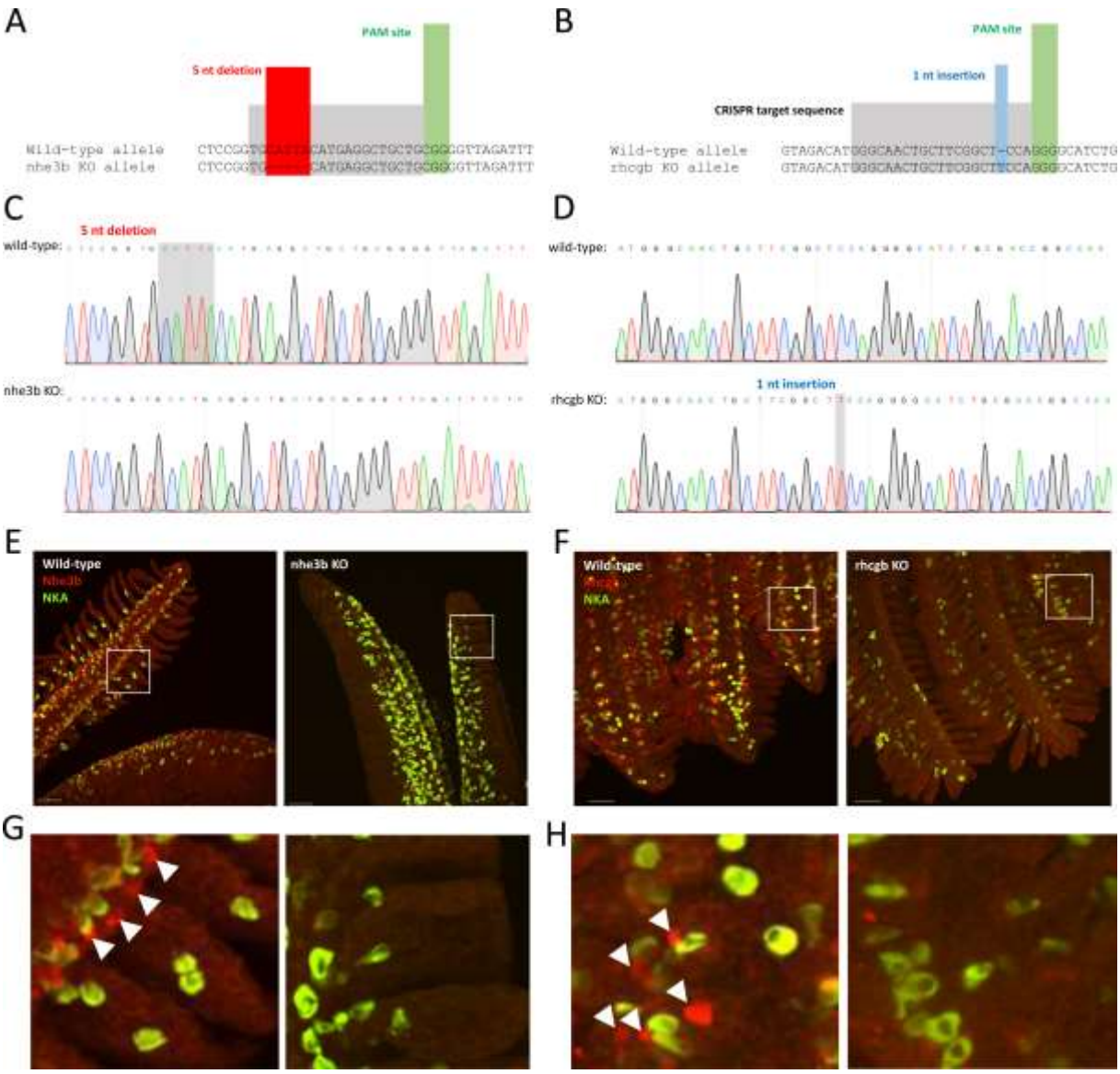

Fig. 1. CRISPR single guide RNA (sgRNA) targets, chromatogram sequences, and whole-mount immunohistochemical knockout confirmation for nhe3b KO and rhcgb KO mutants. Schematic diagram showing CRISPR sgRNA guide target sequences (grey shaded areas), indel mutation sites (red or blue shaded areas), and PAM recognition sites (green shaded areas) for nhe3b KO (A) and rhcgb KO (B) mutants. Chromatogram confirmation of indel mutations in nhe3b KO (C) and rhcgb KO (D) mutants. Whole-mount immunohistochemical staining of adult gills (E-H). Gills of nhe3b KO mutants (E, G) were incubated with anti-Nhe3b (red) and anti-Na^+/K^+-ATPase (green) antibodies. Gills of rhcgb

KO mutants (F, H) were incubated with anti-Rhcgb (red) and anti-Na^+/K^+-ATPase (green) antibodies. Panels G and H are higher magnification views of the regions in white boxes in panels E and F. Scale bars = 50 µm.

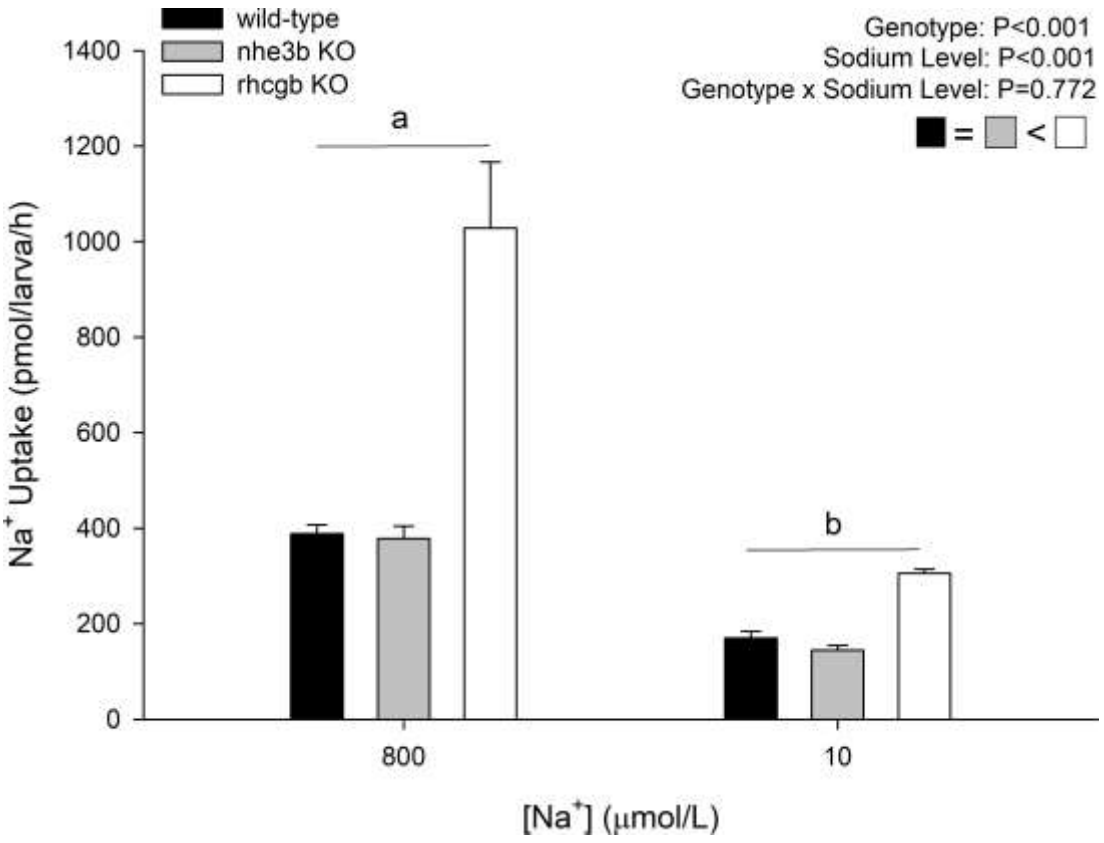

Fig. 2. Na^+ uptake in wild-type, nhe3b KO, and rhcgb KO larvae. Na^+ uptake rates in 4 dpf wild-type (filled bars), nhe3b KO (grey bars), and rhcgb KO (unfilled bars) larvae reared and assayed in 800 (normal) or 10 (low) µmol/L Na^+. Letters above means that differ from one another represent a statistically significant effect of sodium level within a genotype and boxes in the upper right corner of the panel depict the overall statistical effect of genotype as determined by a two-way ANOVA followed by a Holm-Sidak post-hoc test on rank-transformed data. (n = 16 for wild-type means; n = 8 for nhe3b KO and rhcgb KO means)

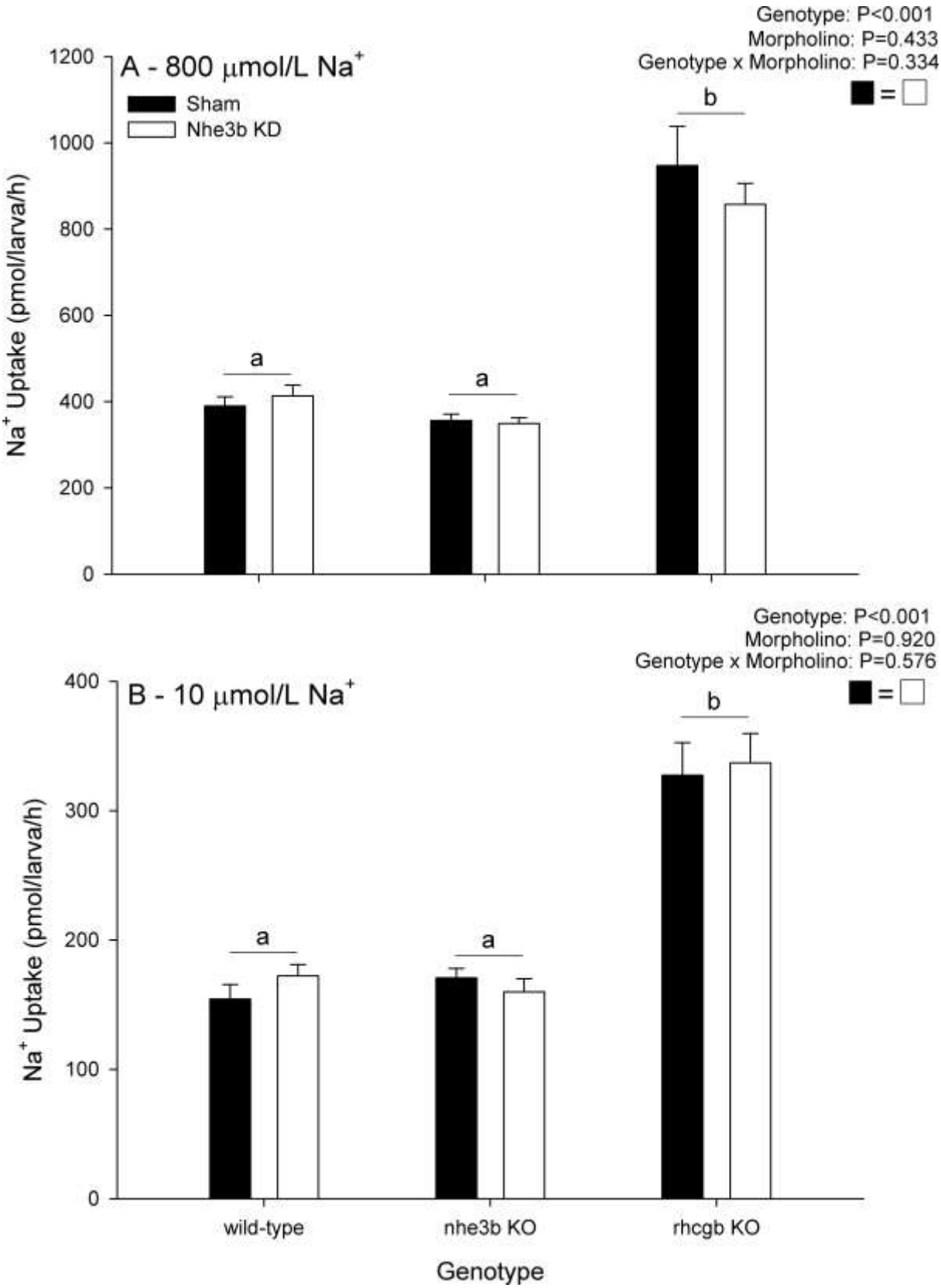

Fig. 3. Na^+ uptake in response to Nhe3b KD in wild-type, nhe3b KO, and rhcgb KO larvae. Na^+ uptake rates in 4 dpf wild-type, nhe3b KO, and rhcgb KO larvae treated with sham (filled bars; Sham) or Nhe3b (unfilled bars; Nhe3b KD) morpholino and reared and assayed in 800 (A) or 10 (B) µmol/L Na^+. Letters above means that differ from one another represent a statistically significant effect of genotype within a morpholino treatment and boxes in the upper right corner of the panels depict the overall statistical effect of morpholino treatment as determined by a two-way ANOVA followed by a Holm-Sidak post-hoc test. (n = 14 - 20)

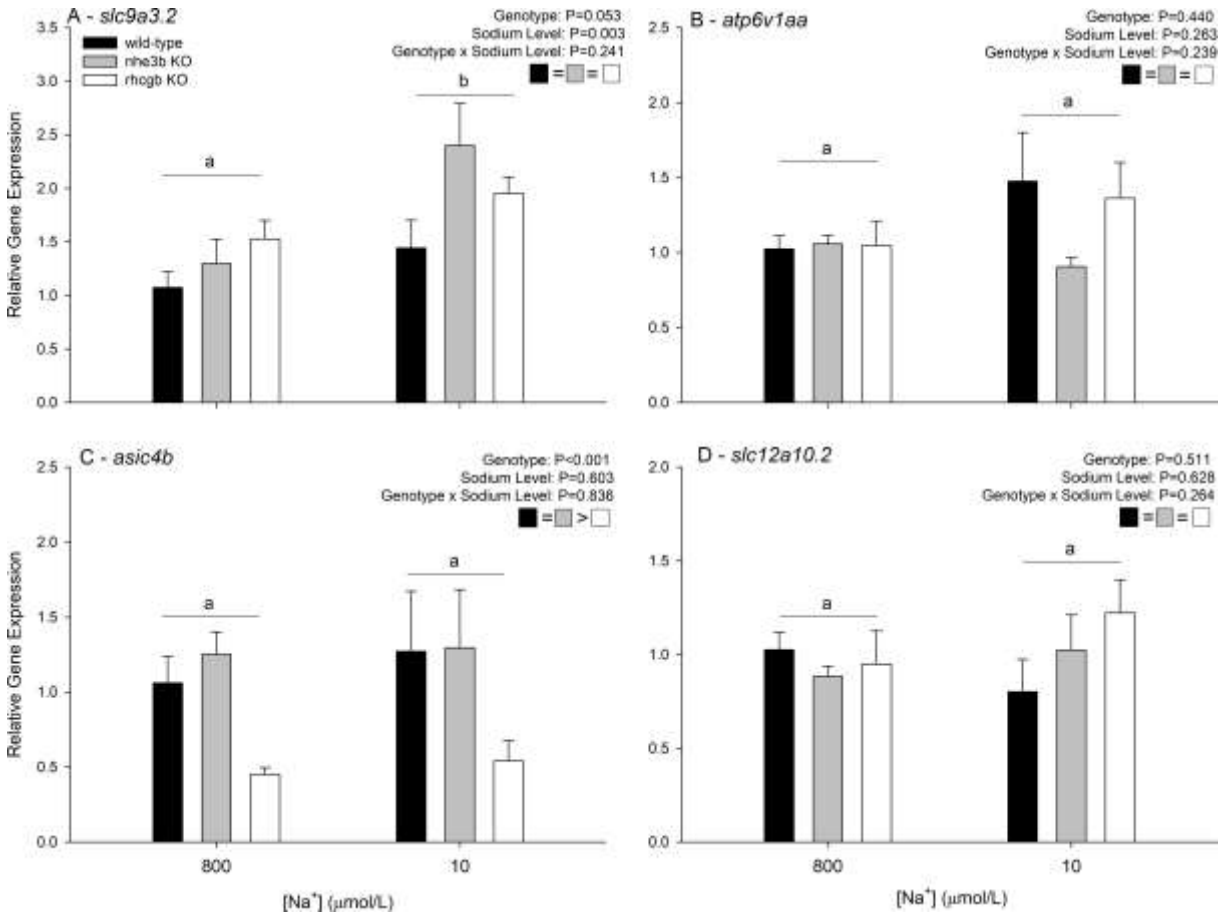

Fig. 4. Whole-body mRNA expression of Na^+ uptake genes in wild-type, nhe3b KO, and rhcgb KO larvae. Relative gene expression (normalized to the expression of *actb2* and expressed relative to wild-types reared in 800 µmol/L Na^+) of s*lc9a3.2* (A; nhe3b), *atp6v1aa* (B; H^+-ATPase), *asic4b* (C), and *slc12a10.2* (D; ncc) in 4 dpf wild-type (filled bars), nhe3b KO (grey bars), and rhcgb KO (unfilled bars) larvae reared in 800 or 10 µmol/L Na^+. Letters above means that differ from one another represent a statistically significant effect of sodium level within a genotype and boxes in the upper right corner of the panels depict the overall statistical effect of genotype as determined by a two-way ANOVA followed by a Holm-Sidak post-hoc test. (n = 5 - 7)

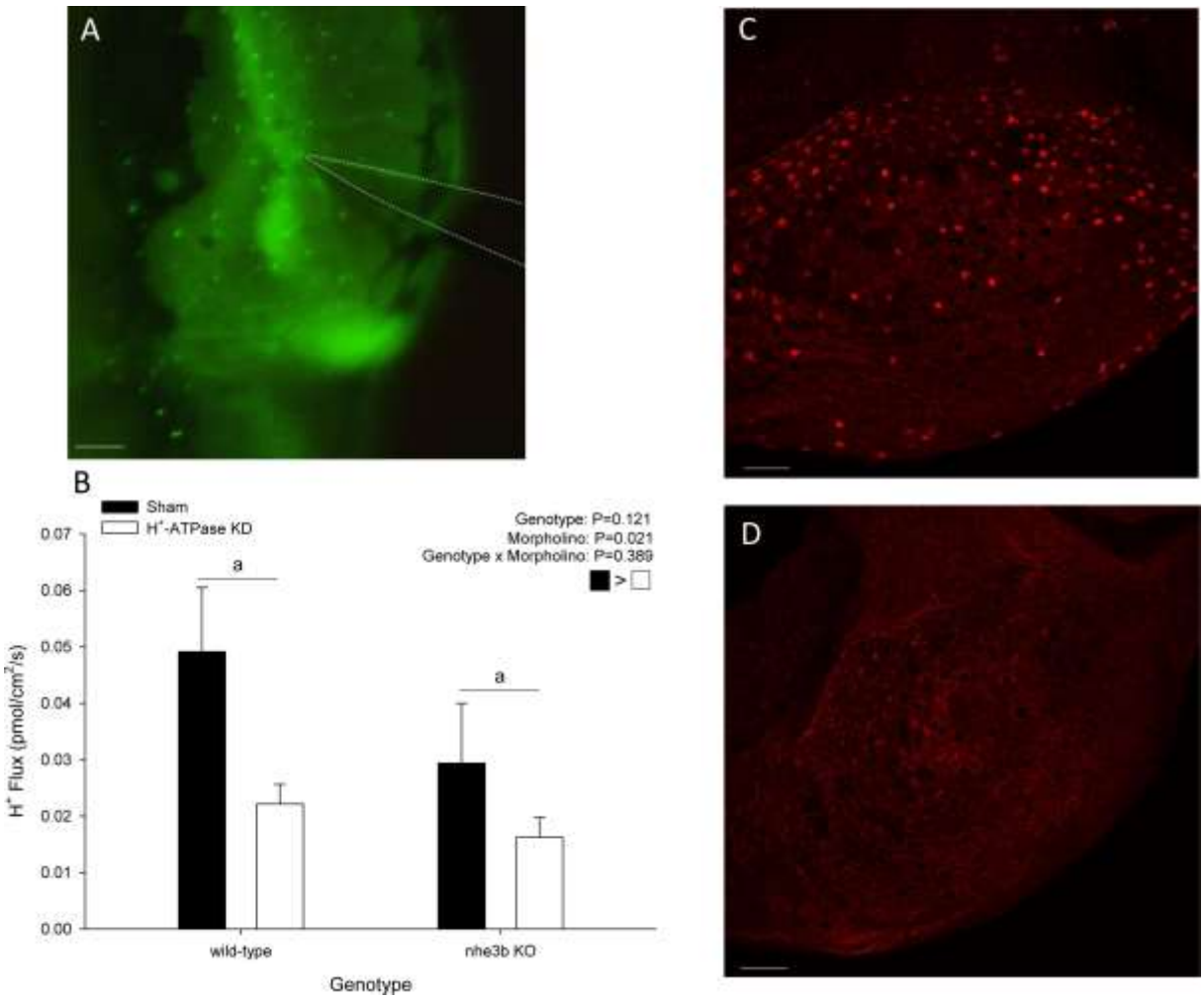

Fig. 5. H^+ fluxes at the surface of HR cells in response to H^+-ATPase KD in wild-type and nhe3b KO larvae. Representative image of a H^+-selective probe positioned above the surface of a HR cell labeled with conA conjugated to Alexa488 (A; scale bar = 50 µm). H^+ flux at the surface of HR cells of 4 dpf wild-type and nhe3b KO larvae treated with sham (filled bars; Sham) or H^+-ATPase (unfilled bars; H^+-ATPase KD) morpholino and reared and assayed in 800 µmol/L Na^+ (B). Letters above means that differ from one another represent a statistically significant effect of genotype within a morpholino treatment and boxes in the upper right corner of the panels depict the overall statistical effect of morpholino treatment as determined by a two-way ANOVA followed by a Holm-Sidak post-hoc test (n = 4 - 5). Immunohistochemical staining of H^+-ATPase in the yolk sac of 4 dpf wild-type larvae treated with sham (C) or H^+-ATPase (D) morpholino (scale bars = 50 µm).

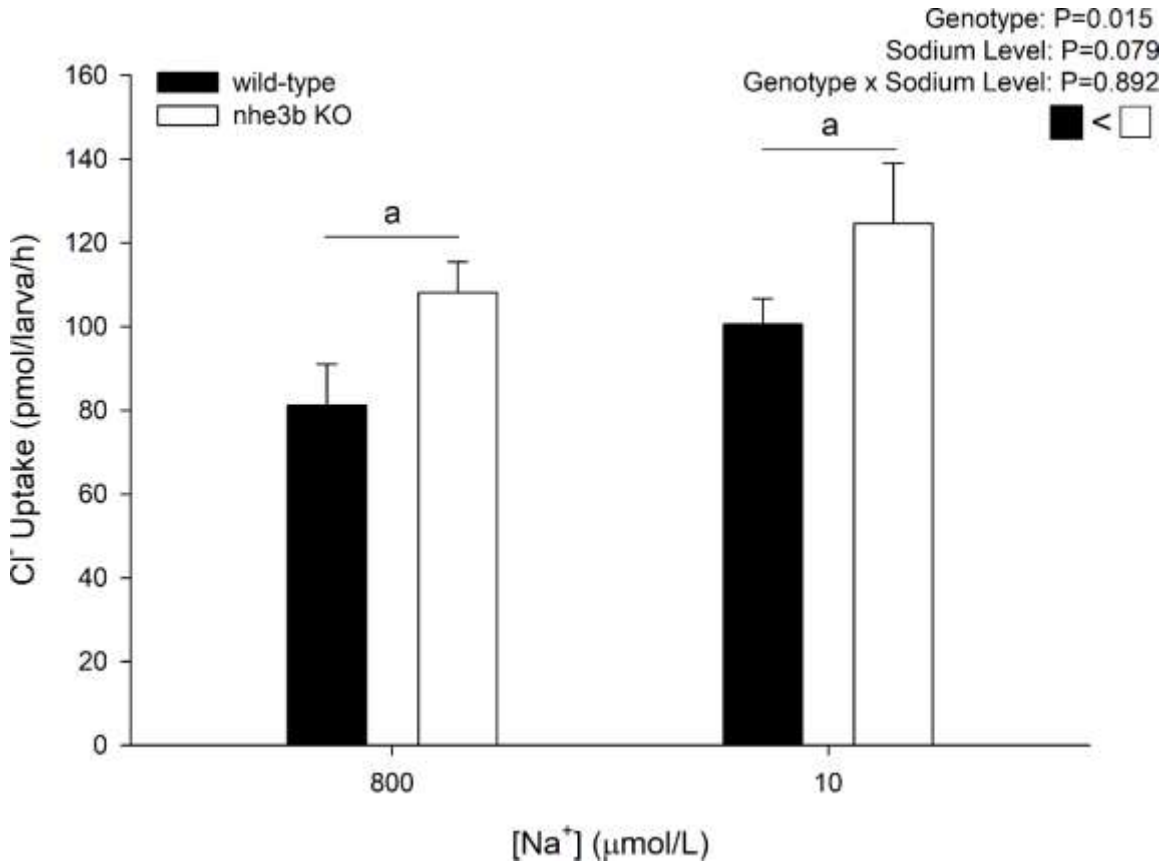

Fig. 6. Cl^- uptake in wild-type and nhe3b KO larvae. Cl^- uptake rates in 4 dpf wild-type (filled bars) and nhe3b KO (unfilled bars) larvae reared and assayed in 800 or 10 µmol/L Na^+. Letters above means that differ from one another represent a statistically significant effect of sodium level within genotype and boxes in upper right corner of the panel depict the overall statistical effect of genotype as determined by a two-way ANOVA followed by a Holm-Sidak post-hoc test. (n = 12)

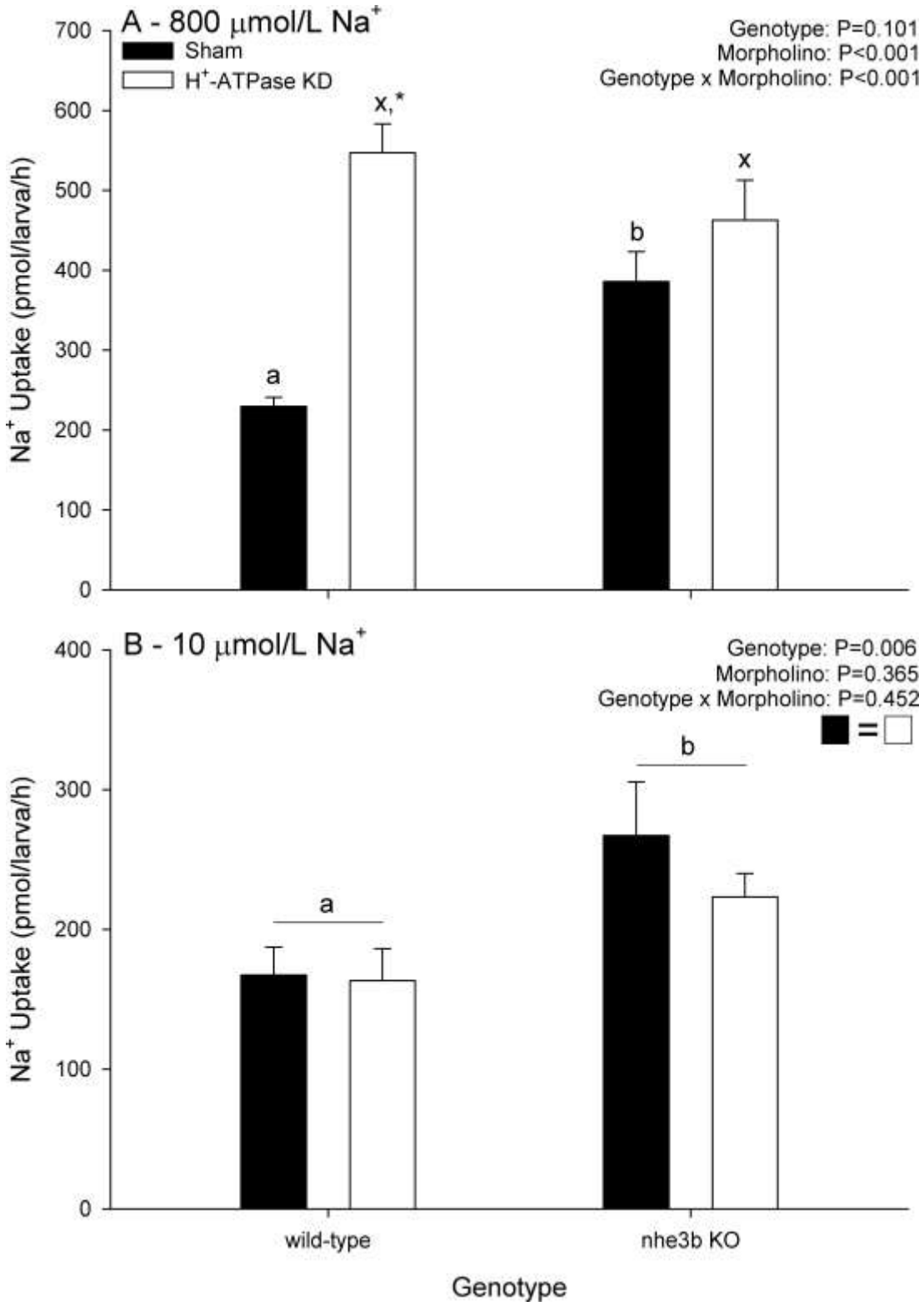

Fig. 7. Na^+ uptake in response to H^+-ATPase KD in wild-type and nhe3b KO larvae. Na^+ uptake rates in 4 dpf wild-type and nhe3b KO larvae treated with sham (filled bars; Sham) or

H^+-ATPase (unfilled bars; H^+-ATPase KD) morpholino and reared and assayed in 800 (A) or 10 (B) µmol/L Na^+. Letters above means that differ from one another represent a statistically significant effect of genotype within a morpholino treatment, asterisks represent a significant effect of morpholino treatment when the interaction term was significant, and boxes in the upper right corner of the panels depict the overall statistical effect of morpholino treatment when the interaction term was not significant as determined by a two-way ANOVA followed by a Holm-Sidak post-hoc test. (A; n = 10 - 14; B; n = 6)

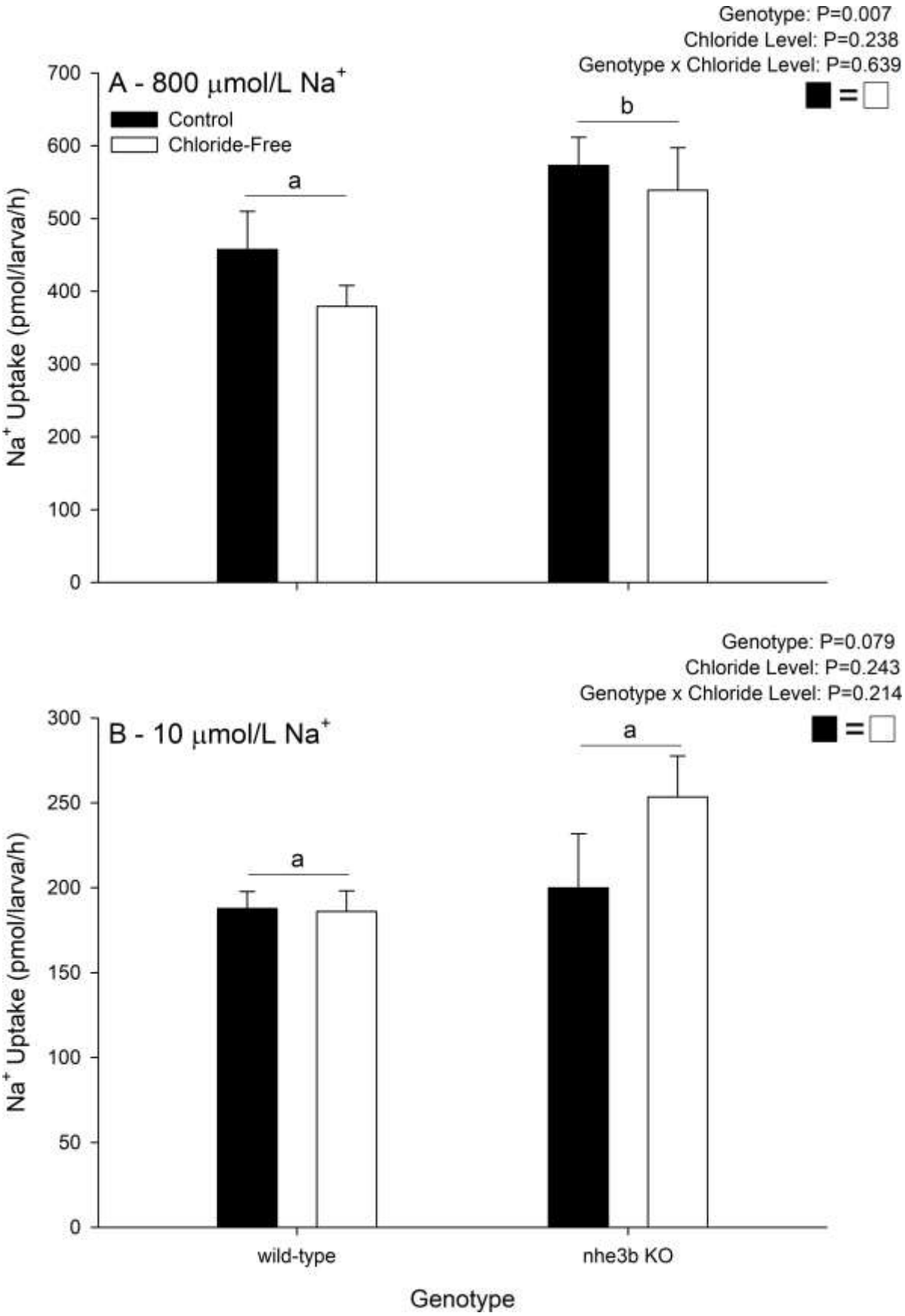

Fig. 8. Na^+ uptake in response to chloride-free conditions in wild-type and nhe3b KO larvae. Na^+ uptake rates in 4 dpf wild-type and nhe3b KO larvae reared and assayed in 800 (A) or 10 (B) µmol/L Na^+ containing 500 (filled bars; Control) or 0 (unfilled bars; Chloride-Free) µmol/L Cl^-. Letters above means that differ from one another represent a statistically significant effect of genotype within chloride treatment and boxes in the upper right corner of the panels depict the overall statistical effect of chloride treatment as determined by a two-way ANOVA followed by a Holm-Sidak post-hoc test. (n = 6)

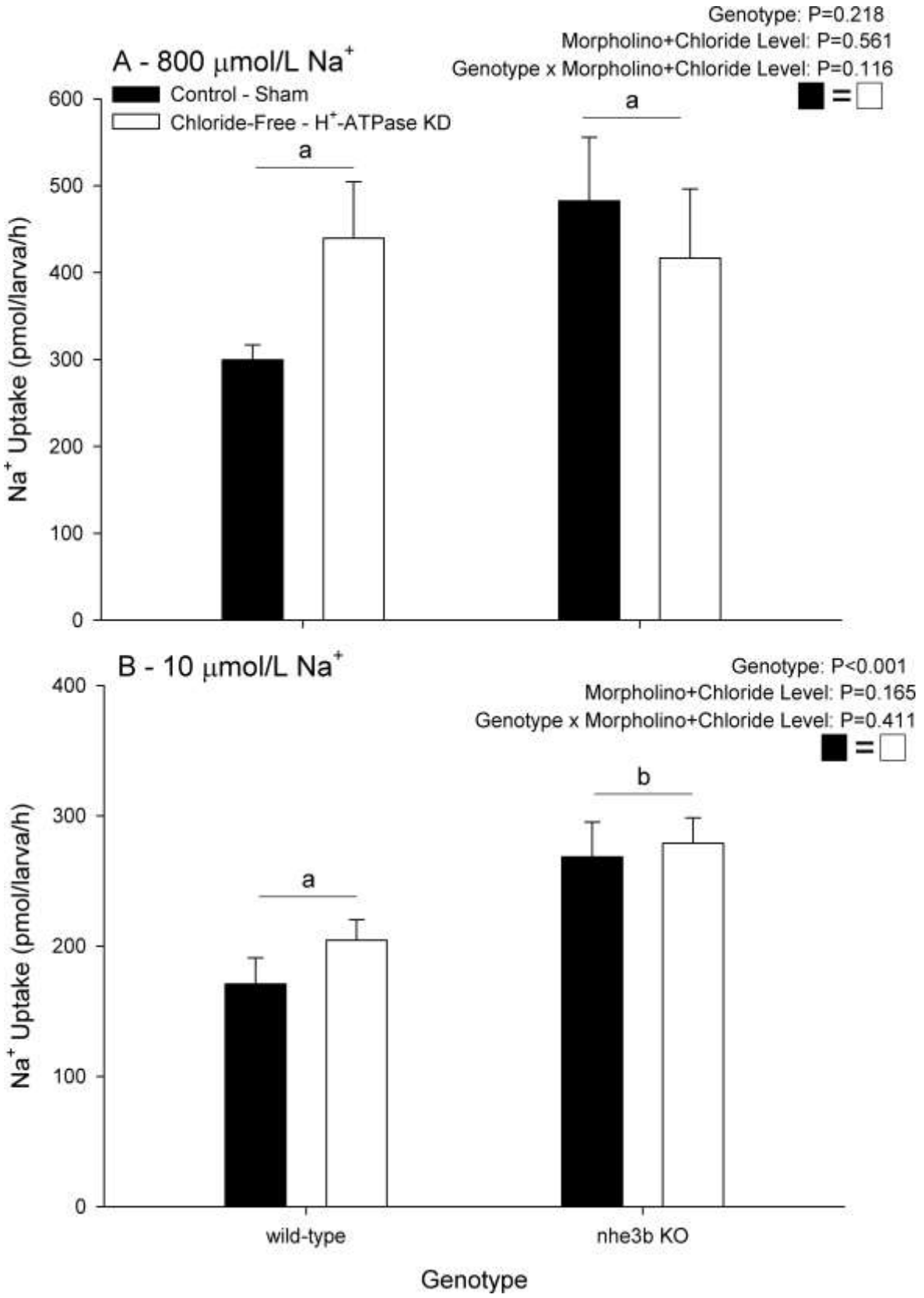

Fig. 9. Na^+ uptake in response to H^+-ATPase KD and chloride-free conditions in wild-type and nhe3b KO larvae. Na^+ uptake rates in 4 dpf wild-type and nhe3b KO larvae treated with sham (filled bars; Sham) or H^+-ATPase (unfilled bars; H^+-ATPase KD) morpholino reared and assayed in 800 (A) or 10 (B) µmol/L Na^+ containing 500 (filled bars; Control) or 0 (unfilled bars; Chloride-Free) µmol/L Cl^-. Letters above means that differ from one another represent a statistically significant effect of genotype within a morpholino + chloride treatment and boxes in the upper right corner of the panels depict the overall statistical effect of morpholino + chloride treatment as determined by a two-way ANOVA followed by a Holm-Sidak post-hoc test. (n = 7 - 8)

Tables

Table 1. Nominal ion concentrations (µmol/L) in reconstituted water used in experimental treatments.

Experimental Treatment	$[Na^+]$ (µmol/L)	$[Cl^-]$ (µmol/L)	$[Ca^{2+}]$ (µmol/L)	$[SO_4^{2-}]$ (µmol/L)	$[K^+]$ (µmol/L)	$[Mg^{2+}]$ (µmol/L)
Normal Na^+/Control Cl^-	800	500	250	550	40	150
Low Na^+/Control Cl^-	10	500	250	155	40	150
Normal Na^+/Cl^--free	800	0	250	800	40	150
Low Na^+/Cl^--free	10	0	250	405	40	150

Table S1. Sequence of the DNA construct used to transcribe the *slc9a3.2* (*nhe3b*) and *rhcgb* single guide RNA (sgRNA), primer sequences used in the generation of the sgRNA DNA construct, and primer sequences used for mutant genotyping. In the DNA construct, underlined nucleotides represent the T7 RNA polymerase promoter, bolded sequence represent the CRISPR/Cas9 target sequence (specific to either *slc9a3.2* or *rhcgb*), and italicized nucleotides represent the Cas9 binding sequence. The two template oligos formed the initial DNA template through partial complementary binding, and the forward and reverse amplification oligos amplified the template.

DNA Construct Sequence	
GCGTAATACGACTCACTATA**NNNNNNNNNNNNNNNNNNN***GTTTTAGAGCTAGAA ATAGCAAGTTAAAATAAGGCTAGTCCGTTATCAACTTGAAAAAGTGGCACCGAGTCGGT GCTTT*	
Primer Name	**Sequence (5'-3')**
slc9a3.2 template oligo	GCGTAATACGACTCACTATATGCATTACATGAGGCTGCTG GTTTTAGAGCTAGAAATAGC
rhcgb template oligo	GCGTAATACGACTCACTATAGGGCAACTGCTTCGGCTCCA GTTTTAGAGCTAGAAATAGC
Universal template oligo	AAGCACCGACTCGGTGCCACTTTTTCAAGTTGATAACGGACT AGCCTTATTTTAACTTGCTATTTCTAGCTCTAAAA
Forward amplification oligo	GCGTAATACGACTCACTATAG
Reverse amplification oligo	AAAGCACCGACTCGGTGCCAC
slc9a3.2 forward sequencing primer	GAAGAACCTCCTGAAACACCAC
slc9a3.2 reverse sequencing primer	TGATAGTGGCAGAATGACTGCT
rhcgb forward sequencing primer	TGTGGCACTTCTTGAAAGTGAT
rhcgb reverse sequencing primer	GCGGGTAAACTGAGTCTGATGT

Table S2. Primers used for real-time PCR.

Name	Sequence (5'-3')	Genbank Accession Number	Reference
actb2 forward	TTACCACTTCACGC CGACTC	NM_131263.1	Present study
actb2 reverse	GTCACCTTCACCGTT CCAGT		
slc9a3.2 forward	TGCAGACAGCGCCT CTAGC	NM_001113479.1	Kwong and Perry (2016)
slc9a3.2 reverse	TGTGGCCTGTCTCTG TTTGC		
atp6v1aa forward	GAGGAACCACTGCC ATTCCA	NM_201135.2	Kwong and Perry (2016)
atp6v1aa reverse	CAACCCACATAAAT GATGACATCG		
asic4b forward	GAACTTGACGTCGG GGTCTT	NM_214786.1	Present study
asic4b reverse	ACCGGTTTCACATG AGGTCC		
slc12a10.2 forward	GCCCCCAAAGTTTT CCAGTT	NM_001045001.1	Kwong and Perry (2016)
slc12a10.2 reverse	TAAGCACGAAGAGG CTCCTTG		

Table S3. Predicted amino acid sequences of nhe3b and rhcgb KO mutants based on Sanger sequencing.

Genotype	Predicted amino acid sequence
nhe3b KO	MAFSTLLLAFLVVSGA*STOP
rhcgb KO	MGNCFGFQGHLRPAKKHQHQTQFTRGVLRLAGVHDHTFRSVCAV*STOP

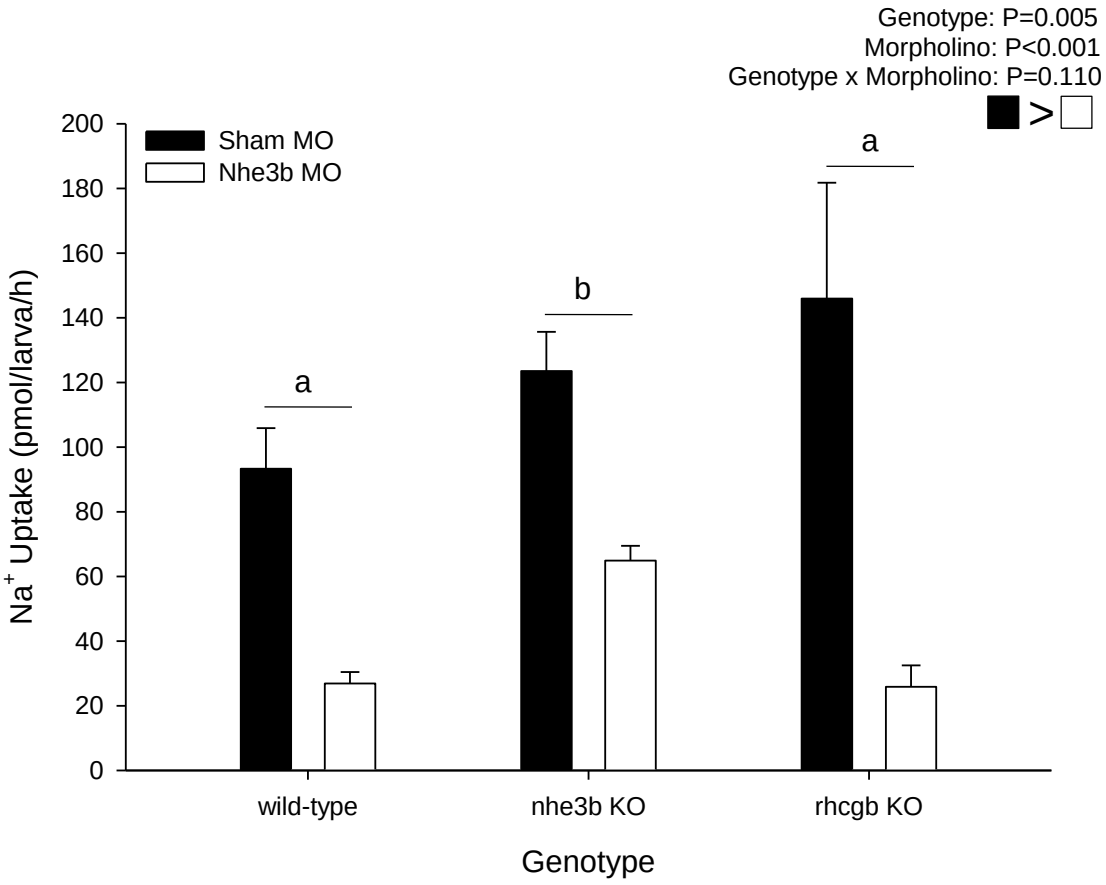

Fig. S1. Na^+ uptake in response to a splice-blocking Nhe3b morpholino in wild-type, nhe3b KO, and rhcgb KO larvae. Na^+ uptake rates in 4 dpf wild-type, nhe3b KO, and rhcgb KO larvae treated with sham (filled bars) or a splice-blocking Nhe3b morpholino (open bars; 5'-GCTCAGTGACTGGAAAGAGAAATA-3'; Kumai and Perry, 2011) morpholino (MO) and reared and assayed in 10 µmol/L Na^+. Letters above means that differ from one another represent a statistically significant effect of genotype within a morpholino treatment and boxes in the upper right corner of the panels depict the overall statistical effect of morpholino treatment as determined by a two-way ANOVA followed by a Holm-Sidak post-hoc test. (n=6-12)